

TITLE PAGE

Lecithin:Cholesterol Acyltransferase Activation by Sulfhydryl-Reactive Small Molecules: Role of Cysteine-31

Lita A. Freeman, Stephen J. Demosky Jr., Monika Konaklieva, Rostislav Kuskovsky,
Angel Aponte, Alice F. Ossoli, Scott M. Gordon, Ross F. Koby, Kelly A. Manthei, Min
Shen, Boris L. Vaisman, Robert D. Shamburek, Ajit Jadhav, Laura Calabresi, Marjan
Gucek, John J.G. Tesmer, Rodney L. Levine, Alan T. Remaley

Primary laboratory of origin: Lipid Metabolism Section, Cardiovascular and
Pulmonary Branch, NHLBI, NIH

Affiliations:

Lipid Metabolism Section, Cardiovascular and Pulmonary Branch, NHLBI, NIH (LAF,
SJD, SMG, BLV, RDS, ATR)

Department of Chemistry, American University (MK, RK)

Systems Biology Center, NHLBI, NIH (AA, MG)

University of Milano, Milano, Italy (AFO, LC)

Department of Chemistry, Vanderbilt University (RFK)

Life Sciences Institute, Departments of Pharmacology and Biological Chemistry,
University of Michigan, Ann Arbor (KAM, JJGT)

NCATS (MS, AJ)

Laboratory of Biochemistry, NHLBI, NIH (RLL)

RUNNING TITLE PAGE

Running Title: *LCAT Activation by Sulfhydryl-Reactive Small Molecules*

Corresponding Author:

Alan T. Remaley

Building 10, Room 2C433

10 Center Dr

Bethesda, MD 20814

Telephone: (301) 402-9796

Email: aremaley1@mail.nih.gov

Number of text pages: 41

Number of tables: 2

Number of figures: 10

Number of references: 50

Number of words in abstract: 250

Number of words in introduction: 845

Number of words in discussion: 1,496

Abbreviations: CE, cholesteryl ester; CER, cholesterol esterification rate; DTNB, dithiobis-nitrobenzoic acid; FC, free cholesterol; FED; fish-eye disease; FLD, familial LCAT deficiency; HDL, high-density lipoprotein; LCAT, lecithin cholesterol acyltransferase; msrA, methionine sulfoxide reductase A; MUP, methylumbelliferyl palmitate; POPC, 1-Palmitoyl-2-oleoyl-*sn*-glycero-3-phosphocholine; rhLCAT, recombinant human LCAT; RMSF, root-mean-square fluctuation.

ABSTRACT

BACKGROUND: Lecithin:cholesterol acyltransferase (LCAT) catalyzes plasma cholesteryl ester formation and is defective in Familial LCAT Deficiency (FLD), an autosomal recessive disorder characterized by low HDL, anemia and renal disease.

OBJECTIVE: To investigate the mechanism by which Compound A, a small heterocyclic amine, activates LCAT. **METHODS:** Effect of Compound A on LCAT was tested in human plasma and with recombinant LCAT. Mass spectrometry and NMR was used to determine Compound A adduct formation with LCAT. Molecular modeling was performed to gain insight into Compound A effects on LCAT structure and activity.

RESULTS: Compound A increased LCAT activity in a subset (3 out of 9) of LCAT mutations to levels comparable to FLD heterozygotes. The site-directed mutation LCAT-Cys31Gly prevented activation by Compound A. Substitution of Cys31 with charged residues (Glu, Arg and Lys) decreased LCAT activity, whereas bulky hydrophobic groups (Trp, Leu, Phe and Met) increased activity up to 3-fold ($p < 0.005$). Mass spectrometry of a tryptic digest of LCAT incubated with Compound A revealed a +103.017 m/z adduct on Cys31, consistent with addition of a single hydrophobic cyanopyrazine ring. Molecular modeling identified potential interactions of Compound A near Cys31 and structural changes correlating with enhanced activity. Functional groups important for LCAT activation by Compound A were identified by testing Compound A derivatives. Finally, sulfhydryl-reactive β -lactams were developed as a new class of LCAT activators. **CONCLUSIONS:** Compound A activates LCAT,

including some FLD mutations, by forming a hydrophobic adduct with Cys31, thus providing a mechanistic rationale for the design of future LCAT activators.

INTRODUCTION

High-density lipoprotein-cholesterol (HDL-C) levels in plasma are inversely related to cardiovascular disease (CVD) risk, but most therapeutic approaches for raising HDL-C in clinical trials have not shown benefit (Rader, 2016). It may be the function rather than the cholesterol content of HDL that accounts for its atheroprotection (Karathanasis et al., 2017). High-density lipoproteins (HDL) are a complex mixture of particles with many different protein and lipid components. Protective functions ascribed to HDL include reverse cholesterol transport from aortic foam cells to the liver, as well as anti-inflammatory, antioxidative, and antiprotease effects (Gordon, 2016; Rosenson et al., 2016; Rye and Barter, 2014). Many of these functions of HDL are performed by larger, spherical particles, so maturation of HDL from small discoidal particles to large spherical particles may be important for CVD protection (Asztalos et al., 2000; Asztalos et al., 2011; Karathanasis et al., 2017).

Lecithin:cholesterol acyltransferase (LCAT), a plasma protein secreted by liver, is an enzyme critical for HDL particle maturation (Ahsan et al., 2014). LCAT catalyzes cholesteryl ester (CE) production from free cholesterol (FC) and phosphatidylcholine (lecithin). Because CEs are more hydrophobic than FC, LCAT activity promotes partitioning of cholesterol from the surface of HDL into its core, converting small discoidal HDL to larger, spherical HDL particles. Moreover, esterification promotes the net egress of cholesterol from cells because unlike FC, CE does not freely equilibrate between cells and lipoproteins. Esterification thereby makes cholesterol efflux to HDL irreversible (Czarnecka and Yokoyama, 1996). Once formed, CE is preferentially delivered to the liver (Schwartz et al., 2004).

CE production by LCAT takes place in two steps. First, LCAT cleaves fatty acids from the *sn*-2 position of phospholipids, using its phospholipase A-2 activity. Ser181, part of the catalytic triad of LCAT (Ser181, Asp345, His377), acts as the nucleophile and is acylated during this step(Ahsan et al., 2014). Next, LCAT transfers the cleaved fatty acid from Ser181 to the A-ring hydroxyl group of cholesterol to produce CE. Phosphatidylcholine is the preferred phospholipid substrate, particularly those with unsaturated fatty acids in the *sn*-2 position(Ahsan et al., 2014).

Recent X-ray crystallographic studies of LCAT confirm the presence of a flexible lid (residues 226-246) that may alter accessibility of the catalytic site to its lipid substrates(Glukhova et al., 2015; Gunawardane et al., 2016; Piper et al., 2015). Certain lid residues (227-DNQGIPVMSS-236) may also contribute to substrate specificity(Glukhova et al., 2015). Residues 36-101 comprise the membrane binding domain of LCAT(Glukhova et al., 2015), with residues 50-74 forming part of the HDL/LDL interfacial binding domain(Adimoolam and Jonas, 1997). LCAT has six cysteines, four in disulfide bonds (Cys50-Cys74 and Cys313-Cys356) that are critical for LCAT activity(Glukhova et al., 2015). The two free cysteines (Cys31 and Cys184) are near the active site, with the Cys31 backbone amide forming part of the oxyanion hole(Glukhova et al., 2015; Holleboom et al., 2011).

Many different LCAT mutations have been described in human patients(Ahsan et al., 2014). The most severe result in familial LCAT deficiency (FLD), characterized by low HDL-C, corneal opacities, anemia, and proteinuria that typically progresses by age 40-50 to end-stage renal disease, the primary cause of morbidity and mortality. LpX, an abnormal multivesicular-like lipoprotein that accumulates in FLD patients, contributes to

their renal disease(Ossoli et al., 2016). Less severe LCAT mutations lead to fish-eye disease (FED), characterized by low HDL-C and corneal opacities but none of the other clinical features of FLD. LCAT is also secondarily decreased in an IL-6-dependent pathway under some conditions(Feister et al., 2002), likely contributing to decreased HDL during inflammation(Khovidhunkit et al., 2004). Decreased LCAT activity has also been observed in “Disappearing HDL Syndrome” in several disorders associated with extremely high levels of IL-10(Moraitis et al., 2015).

We recently developed recombinant human LCAT (rhLCAT) as a potential therapy and showed that it safely increased HDL-C levels in both CAD and FLD patients(Shamburek et al., 2016a; Shamburek et al., 2016b). Because rhLCAT raises HDL and enhances cholesterol efflux, it might protect against CVD, particularly acute coronary syndrome, similar to findings with reconstituted HDL in early-stage clinical trials(Krause and Remaley, 2013; Remaley et al., 2008; Remaley et al., 2014). rhLCAT therapy, however, will likely be relatively expensive and require intravenous infusion. An oral small-molecule activator that increases activity in FLD patients with some residual activity is a possible alternative to rhLCAT therapy and would also be a preferable treatment for CVD. Compound A (3-(5-(ethylthio)-1,3,4-thiadiazol-2-ylthio)pyrazine-2-carbonitrile), the only known small-molecule LCAT activator, was found by Amgen in a high-throughput screen (Kayser et al., 2008) and was shown in hamsters to increase plasma CE and HDL-C levels, hepatic *abcg5/g8* and *cyp7a1* gene expression, and sterol biliary excretion (Chen et al., 2012).

Our objective was to investigate the mechanism for LCAT activation by Compound A and to determine if it can also increase activity of some natural LCAT mutations. We

found that Compound A can indeed activate a subset of FLD mutations by forming a hydrophobic adduct with Cys31 near the active site. We also identified functional groups in Compound A responsible for LCAT activation and describe a new class of LCAT activators based on sulfhydryl-reactive β -lactams. Our findings provide important new mechanistic insights into LCAT activation that can be used to design novel LCAT activators.

METHODS

Cholesterol Esterification Rate - Human plasma for these studies was obtained under informed consent from protocols approved by the NHLBI IRB and the Milano Area C Ethic Committee. Cholesterol esterification rate (CER) was determined by the rate of esterification of [^3H] cholesterol, using 125 μl of plasma samples before and after incubation of plasma at 37°C for 1 h. Before starting the reaction, plasma from subjects with LCAT deficiency carrying different mutations were incubated with Compound A at a final concentration of 10 $\mu\text{g/ml}$. The reaction was stopped with cold ethanol, cholesterol was extracted, and CE was separated from FC by TLC (Dobiasova, 1983; Dobiasova and Schutzova, 1986; Vaisman and Remaley, 2013).

Alternatively, CER was quantitated in some plasma from Italian carriers of LCAT deficiency by measuring FC content before and after incubation of plasma at 37°C for 1 h by an enzymatic colorimetric method (Kempen et al., 2016). A conversion factor between the radioactive and absorbance CER methods was determined by measuring several samples with both methods.

LCAT Plasmid constructs – Human LCAT cDNA was optimized for expression and cloned into pcDNATM4 containing a C-terminal 6-His tag (Glukhova et al., 2015).

Mutants were made using the QuikChange II Site-Directed Mutagenesis kit (Stratagene). Primer sequences are in Supplemental Table S1.

Expression of rhLCAT in tissue culture cells - WT or mutant LCAT plasmid (with C-terminal 6-His tag) was transfected into freshly thawed HEK293 cells, using the TrueFect-Lipo Transfection Reagent (United Biosystems, Herndon, VA) in Opti-MEM media. 24 h later, cells were checked for efficiency of transfection by GFP expression. Media was then changed to serum-free DMEM containing antibiotics, glutamine and 3.75 mM valproic acid sodium salt (Sigma, St. Louis, MO). The conditioned media was removed 48 - 72 h later, centrifuged for 5 min at 500 x g at 4°C and stored frozen at -80°C until use.

Continuous Fluorescence Assay for LCAT - A novel, sensitive fluorescent 96-well plate assay for LCAT, using methylumbelliferyl palmitate (MUP) as a substrate, was developed to measure phospholipase activity of LCAT. The activity was measured by following the increase in fluorescence due to methylumbelliferone formation. Methylumbelliferone (Sigma M-1381), prepared at 100 mM in DMSO and diluted further in PBS, was used to generate standard curves. For apparent K_m and V_{max} calculations, 1 ml of rhLCAT (Rousset et al., 2010) at 50 µg/ml in Assay Buffer (0.1 M sodium phosphate, pH 7.4) was incubated with 2.8 µl of Compound A (10 mg/ml in DMSO) or just DMSO (vehicle) at 37°C for 1 h. 20 µl of each reaction (LCAT minus Compound A, LCAT plus Compound A, or assay buffer) were then added to black 96-well plates (Greiner) in triplicate. During the incubation of LCAT with Compound A, MUP stock (1 mg/ml) was prepared by adding 30 µl Triton X-100 to 1 mg MUP in a glass vial, and then adding DMSO to 1.0 ml. Immediately before use, the MUP stock solution was

diluted in assay buffer to 0, 0.01, 0.02, 0.04, 0.06, 0.1 and 0.15 mM MUP and then 180 μ l of each dilution was immediately added to the wells to start the reaction of LCAT with MUP. LCAT activity (methylumbelliferone formation) was measured by fluorescence at an excitation wavelength of 340 nm and an emission wavelength of 460 nm.

Background due to MUP self-hydrolysis ("assay buffer only" wells) was subtracted from each result. Specific activity (mol MUP hydrolyzed/g LCAT) in conditioned media was determined by dividing mol MUP hydrolyzed by LCAT mass, which was determined by an ELISA (BioVendor, Asheville, NC). Apparent K_m and V_{max} values were calculated using GraphPad Prism software.

Reaction of Compound A with methionine sulfoxide reductase A and glutathione and analysis by mass spectrometry - Recombinant mouse methionine sulfoxide reductase A (msrA) was produced and purified as described (Kim et al., 2010), with the three cysteine residues not at the active site mutated to serine (C107S/C218S/C227S) to avoid complications from oxidation or disulfide formation (Lim et al., 2011). Ten μ l of the modified msrA, at 0.5 mg/ml in 12.5 mM Tris, pH 7.4, was adjusted to 0.1 mg/ml in Compound A by the addition of 0.1 μ l 10 mg/ml Compound A stock solution prepared in dimethylformamide. After 30 min incubation at 37°C, 2 μ l of the reaction was injected onto a reverse phase column with an autosampler set to 4°C (Agilent 1100 series HPLC, Agilent Technologies, Santa Clara, CA). The system contained a Zorbax 300Å StableBond C18 MicroBore column (865630-902, 1.0 x 50mm, 3.5 μ m). The initial solvent was 0.1% formic acid with gradient elution by acetonitrile/0.1% formic acid, increasing at 2%/min with a flow rate of 20 μ L/min. Positive ion electrospray ionization (ESI) mass spectra were obtained with an Agilent 6520 mass spectrometer equipped with a time-of-

flight detector. The capillary voltage was 3500 V, fragmentor voltage was 235 V, nitrogen gas temperature was 350°C, and data was collected in the mass range of 500-2500 m/z. Mass spectra were analyzed and deconvoluted using Agilent software, MassHunter version B.05.

For the reaction of Compound A with glutathione, a solution of 100 µM glutathione was prepared in 50 mM Tris, 1 mM diethylenetriamine-pentaacetic acid, pH 7.5. One µl of 10 mg/ml Compound A in dimethylformamide was added to 99 µl glutathione and incubated at 37°C for 30 min, after which 1 µl was injected into the same HPLC-mass spectrometry system described above. For this analysis, the instrument was run as a tandem mass spectrometer in order to sequence the modified glutathione. The capillary voltage was 3500 V, fragmentor voltage was 175 V, nitrogen gas temperature was 300°C, and the collision cell energy was ramped linearly from 9 to 69 V for the m/z range from 300 to 1500.

NMR analysis of the reaction of Compound 5 (3-((5-(methylthio)-1,3,4-thiadiazol-2-yl)thio)pyrazine-2-carbonitrile) with glutathione (GSH) - To a solution of GSH (Aldrich) (3.3 mg, 10.7 mmol) in 1 ml of D₂O in an NMR tube at room temperature were added 2 ml of dDMF, followed by the addition of (2.86 mg, 10.7 mmol) of Compound 5 (Table 1). The resulting 2:1 dDMF:D₂O solution was left at room temperature for 48 h with occasional shaking. The reaction proceeded cleanly, with no unreacted Compound 5 detected. The reaction resulted in attachment of GSH to the 3rd position of the pyrazine ring of Compound A and departure of the 5-(methylthio)-1,3,4-thiadiazole-2-thiol (thiadiazole ring) as the leaving group.

Reaction of Compound A with LCAT and analysis by mass spectrometry -

Compound A was dissolved in DMSO to a concentration of 10 mg/ml and then diluted to 1.0 mM in PBS, pH 7.4. Next, 1.5 μ l of 1.0 mM Compound A or vehicle was added to 15.0 μ l rhLCAT at 1 mg/ml and incubated at 37°C for 30 min. LCAT, incubated with either vehicle or Compound A, was deglycosylated under denaturing conditions using Protein Deglycosylation Mix (New England Biolabs, Ipswich, MA). To each tube containing 15 μ l rhLCAT, 1.5 μ l H₂O and 2.0 μ l 10X Glycoprotein Denaturing Buffer was added and the reaction was heated at 100°C for 15 min. The reaction was chilled on ice and centrifuged for 10 s. To each tube, 5.0 μ l 10X Glyco2 buffer, 5 μ l 10% NP-40 and 15 μ l H₂O was added. After gentle mixing, 5.0 μ l Deglycosylation Enzyme Cocktail was added. The solution was mixed again and incubated at 37°C for 4 h and then subjected to SDS-PAGE on a 4-12% Bis-Tris NuPAGE gel (Thermo-Fisher Scientific/Invitrogen, Carlsbad, CA) and stained with SimplyBlue (Invitrogen). Gel pieces were destained with 200 mM sodium bicarbonate/40% ACN (1 x 400, 1 x 200 μ l) with frequent vortexing, dried in a Speedvac treated with tributylphosphine and iodoacetamide using the ProteoPrep Reduction and Alkylation Kit (Sigma), washed 2X with 25 mM NH₄CO₃ then 200 μ l NH₄CO₃ in 50% ACN 15 minutes, and then desiccated in a Speedvac.

For trypsin digestion, 20 μ g trypsin (sequencing grade; Promega, Madison, WI) was dissolved in 1.6 ml 25 mM NH₄CO₃ (in H₂O) and enough of the trypsin solution was added to just cover the gel pieces. Gel pieces were rehydrated on ice for 30 min and excess solution was removed. 25 mM NH₄CO₃ was then added to cover the gel pieces. After a brief spin, the samples were placed in a 37°C incubator overnight. After briefly spinning down the gel pieces, the supernatant (containing peptides) was transferred to

a clean tube. Peptides remaining in the gel slices were extracted by incubating the gel pieces, with shaking, in Extraction Buffer (50% acetonitrile, 5% formic acid) at room temperature for 30 min and collecting the supernatant (twice). All three supernatants containing tryptic peptides were then combined, concentrated in a Speedvac, desalted using Ziptips (Millipore, Billerica, MA) and adjusted to 0.1% formic acid. The solution was subjected to analysis by LC/MS on an Orbitrap Fusion coupled with an Ultimate 3000-nLC (Thermo Fisher Scientific). Peptides were separated on an EASY-Spray C₁₈ column (Thermo Scientific; 75 μ m x 25 cm inner diameter, 2 μ m particle size and 100 Å pore size). Separation was achieved by applying a 5–35% linear gradient of acetonitrile plus 0.1% formic acid over 40 min at 300 nl·min⁻¹. An electrospray voltage of 1.9 kV was applied to the eluent via the EASY-Spray column electrode. The Orbitrap Fusion was operated in positive ion data-dependent mode. Full scan MS¹ was performed in the Orbitrap with a normal precursor mass range of 350–1,500 *m/z* at a resolution of 120k. The automatic gain control (AGC) target and maximum accumulation time settings were set to 4 x 10⁵ and 150 ms, respectively. MS² was triggered by selecting the most intense precursor ions above an intensity threshold of 1 x 10³ for collision-induced dissociation (CID)-MS² fragmentation with an AGC target and maximum accumulation time settings of 5 x 10⁴ and 250 ms, respectively. Mass filtering was performed by the quadrupole with 1.2 *m/z* transmission window, followed by CID fragmentation in the Orbitrap at a resolution of 15k and a normalized collision energy (NCE) of 37%. To improve the spectral acquisition rate parallelizable time was activated. The number of MS² spectra acquired between full scans was restricted to a duty cycle of 3 s.

Raw data files were processed with Proteome Discoverer (v1.4, Thermo Fisher Scientific), using Sequest HT search node. Sequest HT searches were performed against SwissProt human database (February 1, 2015). The mass tolerances for parent ions and fragment ions were set as 10 ppm and 0.06 Da, respectively. Trypsin was set as the enzyme and a maximum of two missed cleavages was allowed. Carbamidomethylation of cysteine, methionine oxidation, deamidation (N,Q) and Compound A (103.0269 *m/z*) adduct on cysteine were selected as variable modifications. Peptide spectral matches (PSM) were performed against a target decoy database. PSM's were filtered with a false discovery rate (FDR) cutoff of 1%.

Synthesis of Compound A and derivatives - Methods for synthesis of Compound A (3-(5-(ethylthio)-1,3,4-thiadiazol-2-ylthio)pyrazine-2-carbonitrile) and its derivatives, along with NMR spectra of synthesized compounds are described in Supplemental Materials.

Molecular Modeling – Cholesterol, phospholipid [1-Palmitoyl-2-oleoyl-sn-glycero-3-phosphocholine (POPC)] and Compound A binding to LCAT were modeled using Maestro software (Release 2015-3; Schrodinger). LCAT coordinates from a recent X-ray structure analysis (PDB: 4X96)(Glukhova et al., 2015) were used for molecular docking, using the Glide application. Ligands were docked into the active site of LCAT, using flexible ligand sampling.

To evaluate the influence of Cys31 mutations or Compound A and DNTB adducts on LCAT structure, a high resolution LCAT structure was used (PDB: 4XWG)(Piper et al., 2015). To prepare this structure, the Prime application was used to

replace missing residues 231-237, the Tyr31 mutation was modified back to cysteine, and energy minimization was performed to relax the modified structure. This starting structure was then mutated *in silico* at Cys31 to simulate the various amino acid substitutions or adduct formation by Compound A and DNTB. All-atom molecular dynamics simulations were then performed, using the Desmond application in SPC solvent with 0.15 M NaCl and at a temperature of 310 K. Simulations were run for 20 ns on the NIH High Performance Computing Biowulf Cluster.

All computations for the electrostatic potential of Compound A were run using Gaussian 09 software. Visualizations were made using Gaussview. A 6-31G* basis set was used to optimize the structure and calculate the electrostatic potential of Compound A using the Hartree-Fock method.

Statistical Analysis- Unless otherwise indicated, all results are expressed as the (mean +/- SD) of at least triplicates. Values were compared by a 2-tailed t-test and P-values <0.05 were considered to be statistically significant.

RESULTS

Naturally Occurring LCAT Mutations Activated By Compound A

Compound A and radiolabelled cholesterol were added to plasma from patients bearing different LCAT mutations to measure the CER. Figure 1 shows that Compound A increased LCAT activity in healthy control plasma (WT) by 5 to 6-fold. The M293R LCAT homozygote and the compound LCAT heterozygotes Y312C/E354K and

S91P/A141T had the highest response to Compound A, and reached activity levels that were at least 50% of WT untreated plasma control samples. Two other LCAT mutations, namely K218N and V46E, also showed considerable activation with Compound A, but absolute activity levels of LCAT were still relatively low after Compound A treatment. Mutations near the active site, which had no detectable baseline LCAT activity (R147W and F278S), showed no response to Compound A.

Compound A increases apparent K_m and V_{max} of LCAT by interacting with Cysteine 31

Using methylumbelliferyl palmitate as a substrate to monitor the phospholipase step of the LCAT reaction, we tested the effect of Compound A on the apparent K_m and V_{max} of recombinant LCAT (Fig. 2). Compound A had only a limited effect on the apparent K_m of LCAT but increased the apparent V_{max} by almost 2-fold (control 7.47 +/- 0.26 $\mu\text{M MU}/30$ min; Compound A treatment 14.9 +/- 0.6 $\mu\text{M MU}/30$ min).

It has previously been reported that Cys31 plays a role in modulating LCAT activity (Francone and Fielding, 1991; Gunawardane et al., 2016; Kayser et al., 2008; Piper et al., 2015; Qu et al., 1993). Dithiobis-nitrobenzoic acid (DTNB), a well-known inhibitor of LCAT (Supplemental Fig. 1), forms a mixed disulfide bond with Cys31, resulting in the addition of a nitrobenzoic acid group to Cys31 (Francone and Fielding, 1991). To test whether Compound A, which has three sulfur groups (Table I), may also modulate LCAT activity by covalently reacting with Cys31, we used a codon-optimized full-length human LCAT cDNA tagged with 6-His (Glukhova et al., 2015) and changed Cys31 to glycine (C31G) by site-directed mutagenesis. We also mutated Cys184 to glycine (C184G), because it is the only other free cysteine in LCAT. After transfection

into cells, conditioned media from the cells were tested for LCAT activity, using MUP as the substrate in the presence and absence of Compound A. As can be seen in Figure 3, LCAT-C31G was not activated by Compound A, whereas LCAT-C184G was activated to a similar extent as WT-LCAT.

In Figure 4, we show that replacement of Cys31 with either positively (Arg and Lys) or negatively (Glu) charged amino acids inhibits LCAT activity (Fig. 4), consistent with the proposed mechanism for DTNB inhibition. In contrast, replacement of Cys31 with bulky hydrophobic amino acids (Trp, Tyr, Phe, Leu and Met) resulted in a 2-3 fold activation of LCAT. By comparison, replacement of Cys31 with small polar amino acids (Ser and Thr) or His had a more limited effect (Fig. 4). These combined data are consistent with a model wherein Compound A could activate LCAT by forming a hydrophobic adduct with Cys31.

Compound A alkylates thiols by adding a cyanopyrazine moiety

To explore the reaction of Compound A with proteins containing a free cysteine, we first investigated its effect on a mutated form of mouse msrA, which is 26 kDa in size and contains a single, highly reactive low-pK_a cysteine in its active site (Lim et al., 2012). Compound A was incubated with the mutated msrA and the reaction mixture was analyzed for a mass shift directly without any trypsinization on a QTOF mass spectrometer. The major modified form of msrA found after 30 min exposure to Compound A gained +103.0 Da in mass and was stable to treatment with 25 mM DTT for 90 min. Based on the structure of Compound A, this result is consistent with an

alkylation of the free cysteine of msrA with the cyanopyrazine ring from Compound A (Figure 5A), which is calculated to increase the mass by 103.02 Da.

Figure 5B shows a similar experiment after incubating Compound A with the tripeptide glutathione, which also contains a single highly reactive cysteine. A molar excess of glutathione readily reacted with Compound A to form a derivative with a monoisotopic mass of 410.1021 and another product of mass 177.9710, which is Compound A less the cyanopyrazine moiety. MS/MS of the derivatized glutathione showed a difference of 103.0269 mass units, matching the mass difference in the y₂ ion plus/minus the cyanopyrazine Compound A adduct (Figure 5B).

The reaction of glutathione with Compound 5 (Table 1), a derivative of Compound A that also contains a cyanopyrazine ring and activates LCAT, was monitored by proton NMR (Fig. 6A). The resonance for one of two hydrogens (H_a) on the cyanopyrazine ring, shifted downfield from 8.79 to 8.59 ppm, indicative of a more electron-withdrawing group (S-5-membered thiadiazole ring) in the para position being replaced with a less electron-withdrawing group (Glutathione S). The entire NMR spectrum for this reaction is shown in Supplemental Figure 2 and is consistent with the proposed alkylation reaction of glutathione with the cyanopyrazine ring of Compound A and its derivatives, as shown in the scheme in Figure 6B.

To gain further insight into how Compound A reacts with cysteines, we calculated the relative electrostatic potential of Compound A by the Hartree-Fock method (Fig. 7A,B). The carbon residue (atom C₃, Fig. 7A) in the cyanopyrazine ring that alkylates Cys31 of LCAT was predicted to be the most electropositive part of the molecule

(+0.433) (see also Table 2). This carbon, which is connected to an electron-withdrawing S-thiadiazole group, is also at the end of an alpha-beta unsaturated conjugated π -system due to the presence of the cyano group on the cyanopyrazine ring of Compound A. This likely explains the electropositivity of this site and its susceptibility to nucleophilic attack by reactive cysteine residues in msrA and glutathione. The charges on the analogous carbons in Compound 5 and Compound 10 are similar (+0.414) (Fig. 7C,D; Table 2).

In Figure 8, rhLCAT was incubated with Compound A or vehicle and then deglycosylated, gel-purified and trypsinized. Tryptic peptides were analyzed by LC/MS on an Orbitrap Fusion. In the MS² mode, the monoisotopic m/z of the z=4 LCAT peptide fragments containing Cys31 increased from 640.8445 to 666.5986 after incubation with Compound A (Figures 8A and 8B). This corresponds to a mass difference of 103.0164 Da, nearly identical to the size shift seen with msrA and glutathione after incubation with Compound A. The adduct was present only on LCAT incubated with Compound A and was not detected in LCAT incubated with vehicle. In the MS³ mode, the b₁₆⁺² fragment m/z of the peptide containing Cys31 increased after incubation with Compound A from 844.94153 to 896.45148, or a mass difference of 103.01990 (Figure 8C, D). Consistent with the formation of a cyanopyrazine adduct with an S-C bond rather than a disulfide bond, DTT did not reverse LCAT activation by Compound A (Supplemental Figure 3).

Overall, the combined mass spectrometry and NMR data indicate that the sulfhydryl group of Cys31 of LCAT acts as a nucleophile to attack Compound A, resulting in its alkylation by the attachment of a cyanopyrazine group to the side chain of Cys31.

Molecular Modeling of WT-LCAT Treated with Compound A and LCAT Mutants

Recent X-ray structural analyses of LCAT (Glukhova et al., 2015; Gunawardane et al., 2016; Piper et al., 2015) reveal that Cys31 lies near the catalytic triad active site, with its backbone nitrogen contributing to the oxyanion hole. Therefore, to gain more insight on how WT LCAT and its variants are altered by Compound A, we performed molecular modeling studies.

First, we showed that both LCAT substrates, cholesterol and phosphatidylcholine, were able to dock in the active site of WT LCAT in an orientation that would be expected to promote their catalysis (Supplemental Figures 4A and 4B). Compound A docked in the active site as well, with its cyanopyrazine ring positioned close to the sulfhydryl group of Cys31, which would facilitate their reaction (Supplemental Figure 4C; Fig. 9A). A close-up view of the WT active site docked with phosphatidylcholine also shows how adding a hydrophobic adduct on Cys31 or replacing Cys31 with an amino acid with a hydrophobic side chain could potentially enhance phospholipid binding by increasing hydrophobic interactions with the glycerol backbone of phosphatidylcholine (Fig. 9B).

For LCAT-C31E (Supplemental Figure 4D), which is catalytically inactive, the positively charged choline head group of phosphatidylcholine was predicted to be located near the negative side chain of glutamic acid in position 31 (Supplemental Fig. 4E), thus preventing the proper orientation of the phospholipid substrate for catalysis (compare Supplemental Figure 4D to Supplemental Figure 4B).

Next, we did all-atom molecular dynamics simulations on WT-LCAT and several site-directed mutants, as well as WT-LCAT modified by Compound A and DTNB. The various changes in LCAT structure were made *in silico*, using WT-LCAT as the starting structure, and were then allowed to relax in water at 37°C for 20 ns to reach a stable state (Supplemental Fig. 5). As can be seen in Fig. 10A, the simulation predicted that WT-LCAT undergoes considerable motion in the backbone of the membrane binding domain (residues 36-101), which is adjacent to the active site (Glukhova et al., 2015). Another dynamic region was predicted to be the lid region (residues 225-248) (Fig. 10A), which is near residues in the cap domain that help shape the substrate binding pocket (Glukhova et al., 2015; Piper et al., 2015). When the root-mean-square fluctuation (RMSF) difference in the backbone motion of LCAT modified with Compound A or DTNB versus unmodified LCAT was calculated, several positions within the membrane-binding domain and the lid and substrate binding pocket region showed differential responses to the modifications (Fig. 10B). A similar analysis was performed for various Cys31 mutants (C31M, C31E, C31F, C31L) that either activated or inhibited LCAT (Fig. 4) and a plot correlating the backbone motion with LCAT activity was made (Fig. 10C). This plot showed that areas of increased motion in the membrane binding domain, especially residues 83-90, positively correlate with increased activity. In contrast, increased motion around the lid region, particularly amino acids 238-242, negatively correlated with LCAT activity. Overall, these results suggest that adduct formation by Compound A on LCAT modifies its dynamic structure in particular regions of LCAT that lead to enhanced activity.

Effect of Compound A Derivatives on LCAT activation

To determine the structural requirements of Compound A for LCAT activation, we made and tested several derivatives of Compound A (Table 1).

First, the alkyl substituent of the alkylthio group on the thiadiazole ring of Compound A was changed from an ethyl to a methyl group, forming Compound **5** (Supplemental Figure 6A, Scheme 1). Compound **5** retained LCAT activation but its EC_{50} was increased and its EC_{max} was reduced compared to Compound A (Table 1). Replacement of the thiadiazole ring of Compound A with other groups, such as thiophene (Supplemental Figure 6A, Scheme 1, Compound **6**), as well as substituted benzenes (Supplemental Figure 6A, Scheme 1, Compounds **7**, **8**), negated the ability of these derivatives to activate LCAT. In fact, Compounds **6**, **7**, and **8** were inhibitory at high concentrations ($IC_{50} > 0.06$). This is most likely due to the lack of Lewis bases, such as nitrogen atoms, on the group attached to position 3 of the pyrazine ring. The presence of atoms that are Lewis bases might be necessary for an appropriate positioning of Compound A in close proximity to the Cys31 (Supplemental Figure 7), which is a more likely reason for lack of activity of Compounds **6-8** (Supplemental Figure 6A, Scheme 1) rather than their ability to become good leaving groups.

Compounds substituting the electron-withdrawing CN group on the pyrazine ring of Compound A with CF_3 or NO_2 groups and changing the pyrazine group to pyridine (Supplemental Figure 6B, Scheme 2, Compounds **12-14**), or situating the CN group on the opposite side of the ring as compared to Compound A (Compound **15**) also did not activate LCAT. In fact, Compound **14** was also an inhibitor at high concentrations ($IC_{50} = 6.8 \mu M$ for **14**). Furthermore, alteration of **13** (Supplemental Figure 6B, Scheme 2) by substituting the methylsulfanyl-[1,3,4]thiadiazol-2-ylsulfanyl group with a 4-nitro-

phenylsulfanyl group (**14**, Supplemental Figure 6B, Scheme 2) did not rescue its ability to activate LCAT. The lack of Lewis bases (such as electron-rich nitrogen atoms) as in Compounds **17** and **18** (Supplemental Figure 6C, Scheme 3) led to compounds that were weak inhibitors of LCAT.

Next, we docked Compound A with LCAT to investigate potential interactions with amino acid residues near the active site (Supplemental Fig. 7A, B). The S-ethyl group attached to the thiadiazole ring was predicted to fit into and almost fully occupy a pocket within the substrate binding pocket that contains both hydrophobic and hydrophilic elements (Supplemental Fig. 7A, B). We, therefore, redesigned Compound A by replacing the S-ethyl tail with a propionamide group (Compound **10**, Supplemental Figure 6A, Scheme 1), so that it could potentially form hydrogen bonds with amino acid side chains in the active site (Supplemental Fig. 7C, D). Compound **10**, however, was only a relatively weak activator of LCAT compared to Compound A (Table 1). Upon further inspection, the modeling revealed a potential clash between the propionamide group of Compound 10 with Thr246 (Supplemental Fig. 7C,D), possibly explaining its decreased potency (Table I). Finally, a comparison of the docking of Compound A (Supplemental Figure 7A, B) and Compound 5 (Supplemental Figure 7E, F) with the LCAT active site revealed that Compound A, with its S-CH₂-CH₃ tail, fit into the pocket better than Compound 5, with its shorter S-CH₃ tail, which likely accounts for the superior LCAT activation by Compound A. For all three compounds, Cys31 and Thr248 were shown to interact with electron-rich nitrogen atoms (Lewis bases) in Compound A and its derivatives.

Finally, we synthesized a novel class of thiol-reactive compounds based on monocyclic β -lactams (Compounds **19** and **20**, Table 1; Supplemental Figure 6D, Scheme 4). Both of these compounds contain a methylthio group, which could form a disulfide bond with LCAT by S-methylating Cys31. Because the C31M mutation in LCAT had increased activity (Fig. 4), we predicted that these compounds would activate LCAT. Both of these compounds were nearly good as Compound A in activating LCAT (Table 1). In the case of Compound **19**, LCAT activation could be reversed with DTT, unlike Compound A, consistent with Compound **19** forming an adduct with LCAT by forming of a disulfide bond.

DISCUSSION

A potential clinical indication for small-molecule LCAT activators, such as Compound A, is for the treatment of FLD. We previously investigated the use of rhLCAT as a potential therapy for FLD and found that it was safe and well-tolerated (Shamburek et al., 2016a; Shamburek et al., 2016b). Moreover, rhLCAT treatment almost completely normalized HDL-C levels, improved anemia, and stabilized renal function in a FLD patient with advanced kidney disease (Shamburek et al., 2016a). rhLCAT, however, is an expensive biologic that requires repeated intravenous infusions. A small-molecule treatment approach would be a preferable therapy, if such a drug would activate the LCAT mutations that cause FLD. Compound A has already been shown to increase LCAT activity and raise HDL-C in plasma of mice and hamsters (see (Chen et al., 2012)). We observed, in this study, that three out of nine FLD mutations were activated

by Compound A to a level comparable to FLD heterozygotes. Because FLD heterozygotes are asymptomatic except for their low normal HDL-C levels, these results suggest that small molecule LCAT activators could be a feasible therapeutic approach for a subset of FLD patients, especially since the primary site of action of LCAT is in the plasma.

A second possible clinical indication for small-molecule LCAT activators is for the treatment of CVD. The strong negative correlation between plasma HDL-C levels and CVD risk and the ability of HDL to promote cholesterol efflux from cholesterol-loaded macrophages suggest that HDL-raising therapies might offer protection against CVD. Although some HDL-C raising treatments, such as CETP inhibitors(Karathanasis et al., 2017), have not so far met with success in protecting against CVD, the possible efficacy of LCAT as a CVD therapeutic has not been tested. Studies of the role of LCAT, however, in the pathogenesis of atherosclerosis in both human and animal studies have yielded conflicting results(Ahsan et al., 2014; Rousset et al., 2011). A Mendelian randomization study of subjects with low HDL-C due to LCAT SNPs concluded that low levels of LCAT activity were not associated with an increased risk of CVD(Haase et al., 2012). In contrast, increased levels of pre- β HDL and low LCAT activity have been found in a cohort of patients with CVD(Sethi et al., 2010). In addition, some(Duivenvoorden et al., 2011; Hovingh et al., 2005; van den Bogaard et al., 2012) but not all(Calabresi et al., 2009) FLD heterozygotes appear to have increased carotid atherosclerosis(Ahsan et al., 2014). Moreover, intravenous rhLCAT infusion reduced atherosclerosis in rabbits(Zhou, 2009) and also improved plasma cholesterol efflux and raised plasma HDL-C levels in CVD patients(Shamburek et al., 2016b). If ongoing

clinical trials of rhLCAT demonstrate benefit in reducing atherosclerosis and/or in reducing clinical events in CVD patients, this will likely greatly stimulate efforts to develop small molecule activators of LCAT.

Another major finding from this study is that Compound A forms a hydrophobic adduct with Cys31 of LCAT and increases the apparent V_{\max} of LCAT for at least the first step of the reaction. Site-directed mutagenesis also showed that amino acids with hydrophobic side chains at residue 31 increased LCAT activity, whereas charged amino acid residues, both positive and negative, at the same position, strongly inhibited LCAT. These results are consistent with the qualitative findings for LCAT mutants first reported in the patent for Compound A (Kayser et al., 2008). Replacing Cys31 with Tyr has also been previously described to enhance LCAT activity without significantly altering its structure (Piper et al., 2015). Interestingly, in chickens, the amino acid corresponding to Cys31 in human LCAT is the hydrophobic amino acid phenylalanine (Hengstschlager-Ottstad et al., 1995), and chickens have relatively high plasma levels of HDL-C. Consistent with our observation of decreased activity of the C31E mutation, DTNB, which adds a negatively charged adduct to Cys, is also known to inhibit LCAT (Francone and Fielding, 1991) (Supplemental Figure 1). Mass spectrometry and NMR analysis of msrA and glutathione incubated with Compound A or its derivatives were all consistent with the presence of a hydrophobic cyanopyrazine adduct on the single cysteine in these two model compounds. Finally, mass spectrometry of LCAT incubated with Compound A revealed a +103.016 m/z adduct on the tryptic peptide containing Cys31, thus confirming the addition of a cyanopyrazine ring to Cys31 of LCAT.

Cys31 is located within the active site of LCAT(Glukhova et al., 2015), and therefore it is not unexpected that modification of this residue can affect LCAT activity. Like other interfacial enzymes, LCAT is unable to synthesize CE until it binds to a lipoprotein surface(Ahsan et al., 2014). The interaction with lipoproteins provides the substrates for LCAT but is also predicted to cause the displacement of the lid region that blocks the substrate binding pocket(Ahsan et al., 2014). By our modeling studies, adducts to Cys31 that activate LCAT or site directed mutations in Cys31 that activate LCAT all show increased movement of the membrane binding domain, which may account for the increased LCAT activity after Compound A treatment. Changes in the movement of other regions of LCAT, such as in the lid and substrate binding region, also correlated with changes in activity. From the crystal structures of WT-LCAT(Glukhova et al., 2015) and LCAT-C31Y(Piper et al., 2015), the cavity formed by the substrate binding pocket is relatively large and should be able to readily accommodate adducts at Cys31. As opposed to charge adducts at this position that inhibit LCAT, such as occurs with DTNB, hydrophobic adducts appear to activate LCAT by either promoting the binding of its hydrophobic lipid substrates and/or by promoting a more favorable orientation of the lipid substrate for catalysis. Ongoing efforts to obtain the crystal structure of LCAT modified by Compound A may provide further insight into the mechanism of LCAT activation.

None of the Compound A derivatives that we synthesized showed improvements over the original compound first produced by Amgen in activating LCAT. In fact, many of them turned out to be inhibitors of LCAT at higher concentrations. This may have occurred because Cys31 is in close proximity to the catalytic triad (Ser181, Asp345,

His377), particularly Ser181, which acts as a nucleophile in the first step of the LCAT reaction(Ahsan et al., 2014). This makes preparation of LCAT activators acting at Cys31 challenging, because they will have to be electrophiles that selectively react only with Cys31, and not with the active site serine residue. Alkylating reagents under future consideration should, therefore, be relatively inactive toward oxygen nucleophiles like Ser. The fragment-based synthetic studies that we did on Compound A revealed the importance of the presence of an α, β – unsaturated system (cyanopyrazine ring), as well as the presence of Lewis bases (e.g. nitrogen atoms in the cyanopyrazine ring). The S-ethyl group tail of Compound A also appears to be necessary for appropriately situating the molecule via hydrogen-bonding toward the Cys31 for nucleophilic attack.

A potential limitation of Compound A is that its reaction with glutathione may indicate a lack of specificity. Many drugs that target sulfhydryl groups are in fact non-specific and may react with reactive cysteines on other proteins(Zuniga et al., 2012). There are, however, many examples of sulfhydryl-targeting drugs in current use. Reaction of compound A with LCAT may be somewhat specific, since the reaction with LCAT was complete at 30-60 minutes, whereas reaction of Compound A with glutathione took 48 hours to complete. The Cys31 sulfhydryl in LCAT may be more reactive, possibly due to a lower pKa induced by the effect of neighboring residues in the three-dimensional structure. In general, the rate of reaction of a cysteine is known to be directly proportional to the fraction that is ionized to the thiolate – and that is controlled by the pKa. The excellent fit of Compound A inside the LCAT binding pocket may also add to its specificity for LCAT.

We did succeed in producing a new class of small molecule activators of LCAT based on thiol-reactive β -lactams. Because of their reversibility after DTT treatment, these new compounds likely activate LCAT by forming a mixed disulfide with LCAT by S-methylating Cys31. Again, a limitation of this new class of compounds is that many drugs that target sulfhydryl groups are non-specific and may react with reactive cysteines on other proteins (Zuniga et al., 2012). Previous studies of the N-methylthio class of lactams have shown that the N-S bond is relatively resistant to cleavage by most types of nucleophiles but is susceptible to thiophiles (Shah and Cama, 1987; Woulfe et al., 1985). Moreover, N-thiolated lactams are also known to be non-toxic to mammalian cells (Revell et al., 2007). If the lactam ring of these compounds can be appropriately decorated in order to improve selectivity, perhaps by making it structurally resemble a lipid substrate, it may be possible to make specific LCAT activators based on this class of molecules.

In summary, we describe the mechanism for Compound A activation of LCAT and show that some natural LCAT mutations can be considerably activated by Compound A, thus revealing a possible new treatment strategy for FLD. We also describe a new class of small molecule activators of LCAT based on sulfhydryl-reactive β -lactams. These results provide important new insights into the design of future LCAT activators.

ACKNOWLEDGMENTS

We thank Dr. Tim Hanusa for advice with the Hartree-Fock modeling studies and Dr. Alisa Glukhova for construction of the WT-LCAT-6-His pcDNA4 plasmid.

AUTHORSHIP CONTRIBUTIONS

Participated in research design: Freeman, Demosky, Konaklieva, Kuskovsky, Aponte, Ossoli, Gordon, Koby, Shen, Vaisman, Jadhav, Calabresi, Gucek, Levine, Remaley.

Conducted experiments: Freeman, Demosky, Konaklieva, Kuskovsky, Aponte, Ossoli, Koby, Levine.

Contributed new reagents or analytic tools: Konaklieva, Kuskovsky, Shamburek, Calabresi, Levine.

Performed data analysis: Freeman, Demosky, Konaklieva, Kuskovsky, Aponte, Ossoli, Gordon, Koby, Shen, Jadhav, Levine, Remaley.

Wrote or contributed to the writing of the manuscript: Freeman, Konaklieva, Aponte, Ossoli, Manthei, Tesmer, Levine, Remaley.

Supporting Information: Additional material is online in Supplementary Materials.

REFERENCES

Adimoolam S and Jonas A (1997) Identification of a domain of lecithin-cholesterol acyltransferase that is involved in interfacial recognition. *Biochem Biophys Res Commun* **232**:783-787.

Ahsan L, Ossoli AF, Freeman LA, Vaisman B, Amar MJ, Shamburek RD, and Remaley AT (2014) Role of Lecithin: Cholesterol Acyltransferase in HDL Metabolism and Atherosclerosis, in *The HDL Handbook (Second Edition): Biological Functions and Clinical Implications* (T. Komoda, ed) pp. 159-194, Academic Press.

Asztalos BF, Roheim PS, Milani RL, Lefevre M, McNamara JR, Horvath KV, and Schaefer EJ (2000) Distribution of ApoA-I-containing HDL subpopulations in patients with coronary heart disease. *Arterioscler Thromb Vasc Biol* **20**:2670-2676.

Asztalos BF, Tani M, and Schaefer EJ (2011) Metabolic and functional relevance of HDL subspecies. *Curr Opin Lipidol* **22**:176-185.

Calabresi L, Baldassarre D, Castelnuovo S, Conca P, Bocchi L, Candini C, Frigerio B, Amato M, Sirtori CR, Alessandrini P, Arca M, Boscutti G, Cattin L, Gesualdo L, Sampietro T, Vaudo G, Veglia F, Calandra S, and Franceschini G (2009) Functional lecithin: cholesterol acyltransferase is not required for efficient atheroprotection in humans. *Circulation* **120**:628-635.

Chen Z, Wang SP, Krsmanovic ML, Castro-Perez J, Gagen K, Mendoza V, Rosa R, Shah V, He T, Stout SJ, Geoghagen NS, Lee SH, McLaren DG, Wang L, Roddy TP, Plump AS, Hubbard BK, Sinz CJ, and Johns DG (2012) Small molecule activation of lecithin cholesterol acyltransferase modulates lipoprotein metabolism in mice and hamsters. *Metabolism* **61**:470-481.

Czarnecka H and Yokoyama S (1996) Regulation of cellular cholesterol efflux by lecithin:cholesterol acyltransferase reaction through nonspecific lipid exchange. *J Biol Chem* **271**:2023-2028.

Dobiasova M (1983) Lecithin:cholesterol acyltransferase and the regulation of endogenous cholesterol transport. *Adv Lipid Res* **20**:107-194.

Dobiasova M and Schutzova M (1986) Cold labelled substrate and estimation of cholesterol esterification rate in lecithin cholesterol acyltransferase radioassay. *Physiol Bohemoslov* **35**:319-327.

Duivenvoorden R, Holleboom AG, van den Bogaard B, Nederveen AJ, de Groot E, Hutten BA, Schimmel AW, Hovingh GK, Kastelein JJ, Kuivenhoven JA, and Stroes ES (2011) Carriers of lecithin cholesterol acyltransferase gene mutations have accelerated atherogenesis as assessed by carotid 3.0-T magnetic resonance imaging [corrected]. *J Am Coll Cardiol* **58**:2481-2487.

Feister HA, Auerbach BJ, Cole LA, Krause BR, and Karathanasis SK (2002) Identification of an IL-6 response element in the human LCAT promoter. *J Lipid Res* **43**:960-970.

Francone OL and Fielding CJ (1991) Effects of site-directed mutagenesis at residues cysteine-31 and cysteine-184 on lecithin-cholesterol acyltransferase activity. *Proc Natl Acad Sci U S A* **88**:1716-1720.

Glukhova A, Hinkovska-Galcheva V, Kelly R, Abe A, Shayman JA, and Tesmer JJ (2015) Structure and function of lysosomal phospholipase A2 and lecithin:cholesterol acyltransferase. *Nat Commun* **6**:6250.

Gordon SM and Remaley AT (2017) High density lipoproteins are modulators of protease activity: Implications in inflammation, complement activation, and atherothrombosis. *Atherosclerosis* **259**:104-113.

Gunawardane RN, Fordstrom P, Piper DE, Masterman S, Siu S, Liu D, Brown M, Lu M, Tang J, Zhang R, Cheng J, Gates A, Meininger D, Chan J, Carlson T, Walker N, Schwarz M, Delaney J, and Zhou M (2016) Agonistic Human Antibodies Binding to Lecithin-Cholesterol Acyltransferase Modulate High Density Lipoprotein Metabolism. *J Biol Chem* **291**:2799-2811.

Haase CL, Tybjaerg-Hansen A, Qayyum AA, Schou J, Nordestgaard BG, and Frikke-Schmidt R (2012) LCAT, HDL cholesterol and ischemic cardiovascular disease: a Mendelian randomization study of HDL cholesterol in 54,500 individuals. *J Clin Endocrinol Metab* **97**:E248-256.

Hengstschlager-Ottner E, Kuchler K, and Schneider WJ (1995) Chicken lecithin-cholesterol acyltransferase. Molecular characterization reveals unusual structure and expression pattern. *J Biol Chem* **270**:26139-26145.

Holleboom AG, Kuivenhoven JA, Peelman F, Schimmel AW, Peter J, Defesche JC, Kastelein JJ, Hovingh GK, Stroes ES, and Motzack MM (2011) High prevalence of mutations in LCAT in patients with low HDL cholesterol levels in The Netherlands: identification and characterization of eight novel mutations. *Hum Mutat* **32**:1290-1298.

Hovingh GK, Hutten, BA, Holleboom AG, Petersen W, Rol P, Stalenhoef A, Zwinderman AH, de Groot E, Kastelein JJ, and Kuivenhoven JA (2005) Compromised LCAT function is associated with increased atherosclerosis. *Circulation* **112**:879-884.

Karathanasis SK, Freeman LA, Gordon, SM, and Remaley AT (2017) The Changing Face of HDL and the Best Way to Measure It. *Clin Chem* **63**:196-210.

Kayser F, LaBelle M, Shan B, Zhang J, and Zhou M (2008) Methods for Treating Atherosclerosis U.S. Patent #8426358 (United States: Amgen, Inc.).

Kempen HJ, Gomaraschi M, Simonelli S, Calabresi L, Moerland M, Otvos J, Jeyarajah E, Kallend D, and Wijngaard PL (2016) Persistent changes in lipoprotein lipids after a single infusion of ascending doses of MDCO-216 (apoA-I Milano/POPC) in healthy volunteers and stable coronary artery disease patients. *Atherosclerosis* **255**:17-24.

Khovidhunkit W, Kim MS, Memon RA, Shigenaga JK, Moser AH, Feingold KR, and Grunfeld C (2004) Effects of infection and inflammation on lipid and lipoprotein metabolism: mechanisms and consequences to the host. *J Lipid Res* **45**:1169-1196.

Kim G, Cole NB, Lim JC, Zhao H, and Levine RL (2010) Dual sites of protein initiation control the localization and myristoylation of methionine sulfoxide reductase A. *J Biol Chem* **285**:18085-18094.

Krause BR and Remaley AT (2013) Reconstituted HDL for the acute treatment of acute coronary syndrome. *Curr Opin Lipidol* **24**:480-486.

Lim JC, Gruschus JM, Kim G, Berlett BS, Tjandra N, and Levine RL (2012) A low pKa cysteine at the active site of mouse methionine sulfoxide reductase A. *J Biol Chem* **275**:25596–25601.

Lim JC, You Z, Kim G, and Levine RL (2011) Methionine sulfoxide reductase A is a stereospecific methionine oxidase. *Proc Natl Acad Sci USA* **108**:10472-10477.

Moraitis AG, Freeman LA, Shamburek RD, Wesley R, Wilson W, Grant CM, Price S, Demosky S, Thacker SG, Zarzour A, Hornung RL, Pucino F, Csako G, Yarboro C,

McInnes IB, Kuroiwa T, Boumpas D, Rao VK, Illei GG, and Remaley AT (2015) Elevated interleukin-10: a new cause of dyslipidemia leading to severe HDL deficiency. *J Clin Lipidol* **9**:81-90.

Ossoli A, Neufeld EB, Thacker SG, Vaisman B, Pryor M, Freeman LA, Brantner CA, Baranova I, Francone NO, Demosky SJ Jr., Vitali C, Locatelli M, Abbate M, Zoja C, Franceschini G, Calabresi L, and Remaley AT (2016) Lipoprotein X Causes Renal Disease in LCAT Deficiency. *PLoS One* **11**:e0150083.

Piper DE, Romanow WG, Gunawardane RN, Fordstrom P, Masterman S, Pan O, Thibault ST, Zhang R, Meininger D, Schwarz M, Wang Z, King C, Zhou M, and Walker NP (2015) The high-resolution crystal structure of human LCAT. *J Lipid Res* **56**:1711-1719.

Qu SJ, Fan HZ, Blanco-Vaca F, and Pownall HJ (1993) Roles of cysteines in human lecithin:cholesterol acyltransferase. *Biochemistry* **32**:3089-3094.

Rader DJ (2016) New Therapeutic Approaches to the Treatment of Dyslipidemia. *Cell Metab* **23**:405-412.

Remaley AT, Amar M, and Sviridov D (2008) HDL-replacement therapy: mechanism of action, types of agents and potential clinical indications. *Expert Rev Cardiovasc Ther* **6**:1203-1215.

Remaley AT, Norata GD, and Catapano AL (2014) Novel concepts in HDL pharmacology. *Cardiovasc Res* **103**:423-428.

Revell KD, Heldreth B, Long TE, Jang S, and Turos E (2007) N-thiolated beta-lactams: Studies on the mode of action and identification of a primary cellular target in *Staphylococcus aureus*. *Bioorg Med Chem* **15**:2453-2467.

Rosenson RS, Brewer HB Jr, Ansell BJ, Barter P, Chapman MJ, Heinecke JW, Kontush A, Tall AR, and Webb NR (2016) Dysfunctional HDL and atherosclerotic cardiovascular disease. *Nat Rev Cardiol* **13**:48-60.

Rousset X, Shamburek R, Vaisman B, Amar M, and Remaley AT (2011) Lecithin cholesterol acyltransferase: an anti- or pro-atherogenic factor? *Curr Atheroscler Rep* **13**;
249-256.

Rousset X, Vaisman B, Auerbach B, Krause BR, Homan R, Stonik J, Csako G, Shamburek R, and Remaley AT (2010) Effect of recombinant human lecithin cholesterol acyltransferase infusion on lipoprotein metabolism in mice. *J Pharmacol Exp Ther* **335**:140-148.

Rye KA and Barter PJ (2014) Cardioprotective functions of HDLs. *J Lipid Res* **55**:168-179.

Schwartz CC, VandenBroek JM, and Cooper PS (2004) Lipoprotein cholesteryl ester production, transfer, and output in vivo in humans. *J Lipid Res* **45**:1594-1607.

Sethi AA, Sampson M, Warnick R, Muniz N, Vaisman B, Nordestgaard BG, Tybjaerg-Hansen A, and Remaley AT (2010) High pre-beta1 HDL concentrations and low lecithin: cholesterol acyltransferase activities are strong positive risk markers for ischemic heart disease and independent of HDL-cholesterol. *Clin Chem* **56**:1128-1137.

Shah NV and Cama LD (1987) Synthesis of a Novel Carbapenem-Potassium (5r,6r)-1,1-Difluoro-2-Phenyl-6-(1r-Hydroxyethyl)-Carbapen-2-Em-3-Carboxylate - the Use of a New N-Protecting Group in Beta-Lactam Synthesis. *Heterocycles* **25**:221-227.

Shamburek RD, Bakker-Arkema R, Auerbach BJ, Krause BR, Homan R, Amar MJ, Freeman LA, and Remaley AT (2016a). Familial lecithin:cholesterol acyltransferase deficiency: First-in-human treatment with enzyme replacement. *J Clin Lipidol* **10**:356-367.

Shamburek RD, Bakker-Arkema R, Shamburek AM, Freeman LA, Amar MJ, Auerbach B, Krause BR, Homan R, Adelman SJ, Collins HL, Sampson M, Wolska A, and Remaley AT (2016b) Safety and Tolerability of ACP-501, a Recombinant Human Lecithin:Cholesterol Acyltransferase, in a Phase 1 Single-Dose Escalation Study. *Circ Res* **118**:73-82.

Vaisman BL and Remaley AT (2013) Measurement of lecithin-cholesterol acyltransferase activity with the use of a peptide-proteoliposome substrate, in *Lipoproteins and Cardiovascular Disease: Methods and Protocols* Methods Mol Biol (Freeman LA ed) pp. 343-352, Springer, New York

van den Bogaard B, Holleboom AG, Duivenvoorden R, Hutten BA, Kastelein JJ, Hovingh GK, Kuivenhoven JA, Stroes ES, and van den Born BJ (2012) Patients with low HDL-cholesterol caused by mutations in LCAT have increased arterial stiffness. *Atherosclerosis* **225**:481-485.

Woulfe SR, Iwagami H, and Miller MJ (1985) Efficient N-Sulfenylation of 2-Azetidinones Using S-Substituted Thiophthalimides. *Tetrahedron Lett* **26**:3891-3894.

Zhou M (2009) Lecithin Cholesterol Acyltransferase Promotes Reverse Cholesterol Transport and Attenuates Atherosclerosis Progression in New Zealand White Rabbits Paper presented at: Circulation.

Zuniga FI, Loi D, Ling KH, and Tang-Liu DD (2012) Idiosyncratic reactions and metabolism of sulfur-containing drugs. *Expert Opin Drug Metab Toxicol* **8**:467-485.

FOOTNOTES

Funding Source Statement: This research was supported in part by the Intramural Research Program of the National Institutes of Health (NHLBI and NCATS). This work was also supported by National Institutes of Health grants [HL071818] and [HL122416] (to J.T.), and an F32 Ruth L. Kirschstein National Research Service Award [F32HL131288] to K.A.M.

LEGENDS FOR FIGURES

Figure 1: Compound A increases LCAT plasma activity for some LCAT mutations.

Cholesterol esterification rate (CER) was determined in plasma of FLD and FED patients using either (A) the ^3H CER method or (B) the CER enzymatic absorbance method. FLD mutations were T274I, R147W, K218N and F278S. FED mutations were V46E, Y312C/E354K and S91P/A141T. Results represent mean \pm SD of at least triplicates. * ($p < 0.05$) compared to untreated control.

Figure 2: Compound A increases the apparent V_{\max} of LCAT.

rhLCAT was incubated with Compound A or vehicle. LCAT activity (100 ng LCAT/well in all reactions) was then measured by following methylumbelliferone (MU) formation at 460 nm after 30 min in the presence of increasing concentrations of the substrate, methylumbelliferyl palmitate (MUP). Results represent mean \pm SD of at least triplicates. ** ($p < 0.02$) compared to WT-LCAT treated under the same conditions.

Figure 3: Cys31 is required for activation of LCAT by Compound A.

Conditioned media from cells transfected with WT-LCAT (Glukhova et al., 2015) and C31G and C184G mutants were incubated with the indicated concentrations of Compound A (x-axis), and then tested for LCAT activity with MUP as the substrate. Results are normalized to untreated activity levels for each LCAT variant. Results represent mean \pm SD of at least triplicate measurements. *** ($p < 0.005$) compared to WT-LCAT treated under same conditions.

Figure 4: Charged residues at position 31 inhibit and hydrophobic residues activate LCAT. Comparison of LCAT-specific activity of WT (Cys31) versus site-directed mutants at position 31 (x-axis). Conditioned media from HEK293 cells transfected with WT or mutant LCAT plasmids were collected and assayed for LCAT mass by ELISA and activity using MUP as the substrate. Results represent mean +/- SD of at least triplicate measurements. * ($p < 0.02$); ** ($p < 0.005$) compared to WT-LCAT.

Figure 5: Mass spectrometry analysis of msrA- and glutathione-Compound A adducts. (A) Scheme for the reaction of the single cysteine residue on msrA with Compound A. The major modified form of msrA gained +103.0 Da in mass, consistent with addition of the cyanopyrazine ring from Compound A to the free cysteine of msrA. (B) MS-MS spectrum of the glutathione cysteine reaction product demonstrates a cyanopyrazine ring. A molar excess of glutathione reacted readily with Compound A to form a derivative with a monoisotopic mass of 410.1021 and another product of mass 177.9710, which has the same mass as Compound A less the cyanopyrazine moiety (see Fig. 5A). Boxes indicate position of various mass fragment ions from the reaction.

Figure 6: NMR analysis of Compound 5-Glutathione adduct. (A) NMR spectra (left) of region corresponding to two hydrogen groups (H_a and H_b) of Compound 5 before (top), mid reaction (24 h) (middle panel) and after completion of reaction (48 h) (bottom) with glutathione, showing a shift in the spectra for H_a after derivitization with glutathione. (B) Scheme for reaction mechanism of glutathione with Compound A. Carbon # 3 of Compound A (FW 281.38) undergoes nucleophilic attack by the free sulfhydryl group of Glutathione-SH (FW 307.32), leading to a Compound A-glutathione adduct of 410.1008 m/z.

Figure 7: Electrostatic Potential Map of Compounds A, 5 and 10. (A) Charge distribution of Compound A, numbered ball and stick view. Atomic charges on carbon (gray) and sulfur (yellow), are shown. Nitrogen atoms are shown in teal. Units for the atomic charge are relative units to the total charge of the molecule. (B) Electrostatic potential map of Compound A. Blue shows electronegativity and red shows electropositivity. (C,D) Charge distribution of Compound 5 (C) or Compound 10 (D), numbered ball and stick view, as in (A).

Figure 8: Mass spectrometry analysis of LCAT treated with Compound A. MS² spectra of LCAT before (A) and after (B) treatment with Compound A. Peaks correspond to precursor ions of the deamidated LCAT peptide AELSnHTRPVILVPGCLGNQLEAK, containing Cys31. *: monoisotopic peak. (B) MS³ spectra produced by collision-induced dissociation (CID) of the (M + 4H)⁴⁺ precursor ions of the deamidated peptide AELSnHTRPVILVPGCLGNQLEAK, containing Cys31 before (C) and after (D) treatment with Compound A. Arrow indicates fragmentation position of LCAT peptide to produce the b₁₆⁺² fragment.

Figure 9: Molecular modeling of WT-LCAT active site. (A) WT-LCAT was docked with Compound A in its active site, showing the close position of Cys31 near the cyanopyrazine ring of Compound A. (B) WT-LCAT was docked with POPC in its active site, showing the close position of Cys31 near the hydrophobic glycerol backbone of POPC. His377 and Ser181 of the catalytic triad are shown as well.

Figure 10: Molecular dynamics simulations of LCAT reveal backbone motion. (A) Root mean square fluctuation (RMSF) (in Å) for WT LCAT compared to the starting

structure at each position in the LCAT sequence. (B) The Delta RMSF of WT LCAT modified either with DTNB (green) or Compound A (red) was calculated as the difference from the RMSF of WT LCAT. (C) Correlation between Delta RMSF with LCAT activity, with a positive slope corresponding to protein regions in which increased backbone motion is associated with increased LCAT activity. Amino acid residues in the membrane binding domain (36-101) and the cap domain containing the lid (residues 226-246), as well as residues that help shape the substrate binding pocket (Glukhova et al., 2015; Piper et al., 2015), are shown below the x-axis.

Table 1

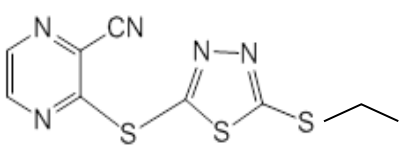
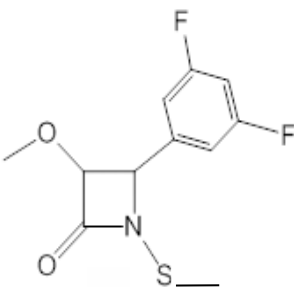
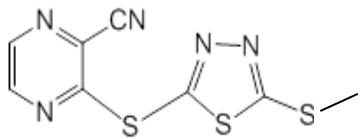
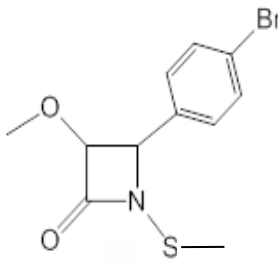
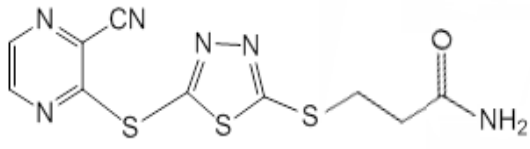
<p>Compound A</p>  <p>3-((5-(ethylthio)-1,3,4-thiadiazol-2-yl)thio)pyrazine-2-carbonitrile</p> <p>EC₅₀ (mM) 0.794 EC_{Max} (%) 161.3</p>	<p>Compound 19</p>  <p>(±) (3S,4R)-4-(3,5-Difluorophenyl)-3-methoxy-1-(methylthio)azetidin-2-one</p> <p>EC₅₀ (mM) 1.69 EC_{Max} (%) 167.3</p>
<p>Compound 5</p>  <p>3-((5-(methylthio)-1,3,4-thiadiazol-2-yl)thio)pyrazine-2-carbonitrile</p> <p>EC₅₀ (mM) 5.81 EC_{Max} (%) 149.6</p>	<p>Compound 20</p>  <p>(±) (3S,4R)-4-(4-Bromophenyl)-3-methoxy-1-(methylthio)azetidin-2-one</p> <p>EC₅₀ (mM) 1.02 EC_{Max} (%) 165.4</p>
<p>Compound 10</p>  <p>3-[5-(3-cyano-pyrazin-2-ylsulfanyl)-[1,3,4]thiadiazol-2-ylsulfanyl]-propionamide</p> <p>EC₅₀ (mM)* 142 mM* EC_{Max} (%) 135.6* *Calculated at highest dose *Did not reach maximum</p>	

Table 1: Structure of Compound A and other LCAT activators. EC₅₀ and EC_{max} are shown for (left) Compound A and derivatives (Compounds 5, 10); and (right) the β-lactam-based Compound 19 and Compound 20.

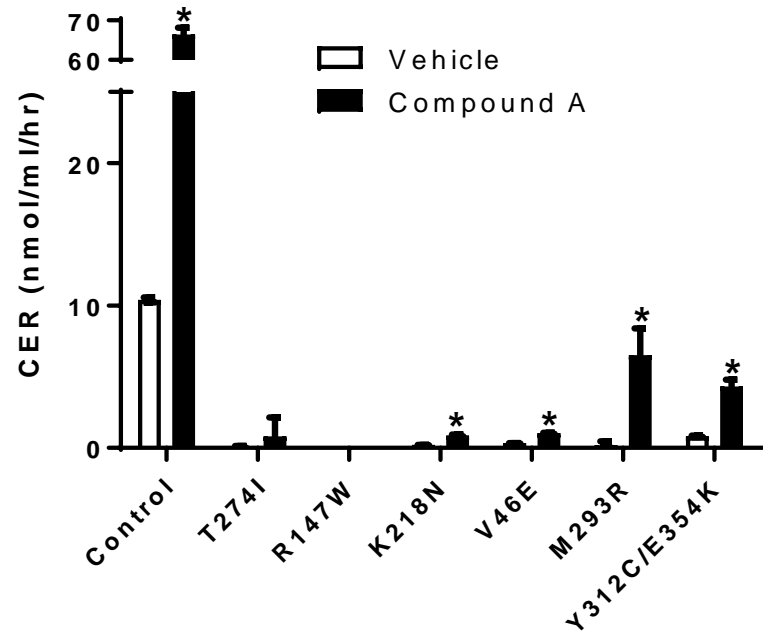
Table 2

Atom (Charge distribution numbering)	Atomic Charge		
	Compound A	Compound 5	Compound 10
N ₁	-0.45	-0.448	-0.449
C ₁	0.318	0.307	0.307
C ₂	0.217	0.243	0.241
C ₃	0.433	0.414	0.414
N ₂	-0.484	-0.482	-0.481
C ₄	0.229	0.234	0.226
C ₅	0.099	0.1	0.104
N ₃	-0.382	-0.391	-0.39
S ₁	-0.203	-0.198	-0.193
C ₆	0.373	0.397	0.379
N ₄	-0.364	-0.396	-0.379
N ₅	-0.262	-0.207	-0.224
C ₇	0.373	0.348	0.395
S ₂	-0.011	-0.029	-0.03
S ₃	-0.268	-0.183	-0.245
C ₈	0.152	-0.144	-0.157
C ₉	0.076		0.197
C ₁₀			0.777
N ₆			-1.079
O ₁			-0.61

Table 2: Atomic charge from electrostatic potential of individual atoms of Compound A, Compound 5 and Compound 10. Charge distribution for carbon, nitrogen and sulfur atoms of Compounds A, 5 and 10 are shown. Units for the atomic charge are relative units to the total charge of the molecule. See Figure 7 for compound numbering schemes.

Figure 1

A



B

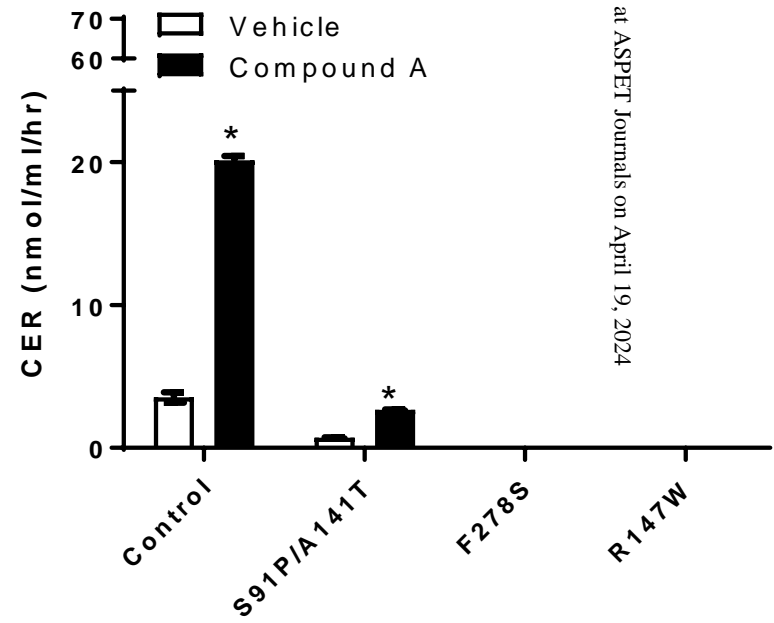


Figure 2

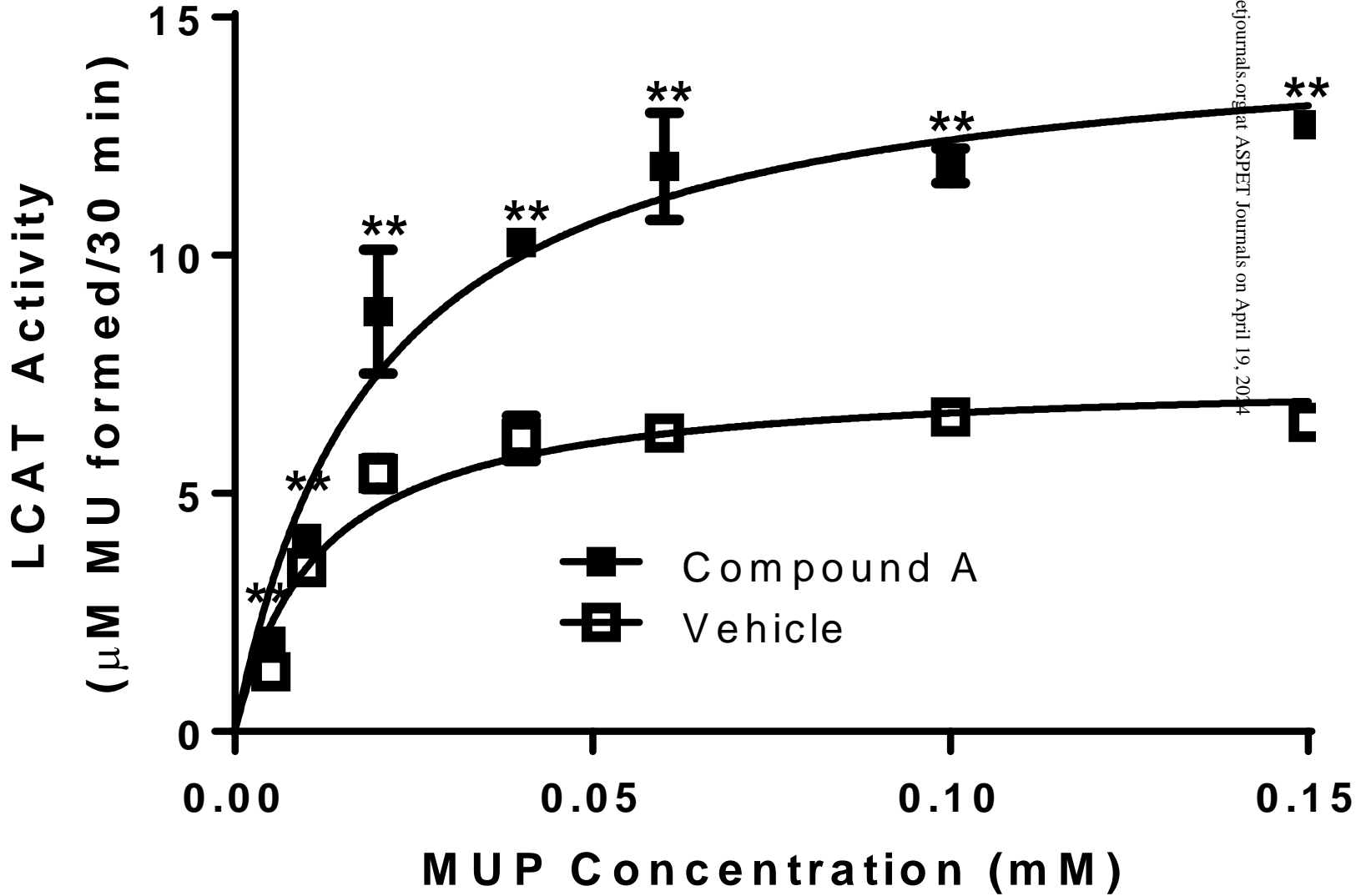


Figure 3

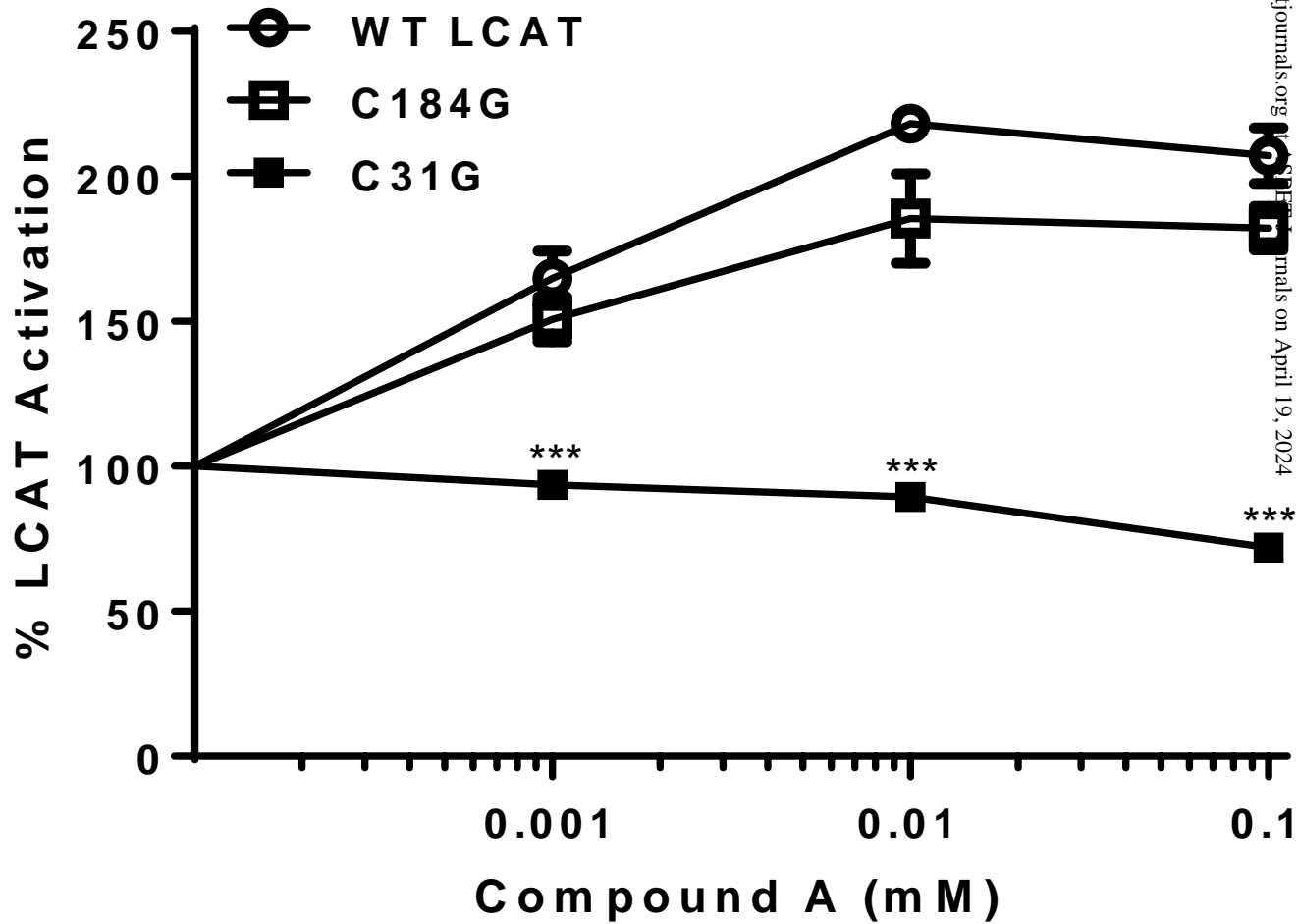


Figure 4

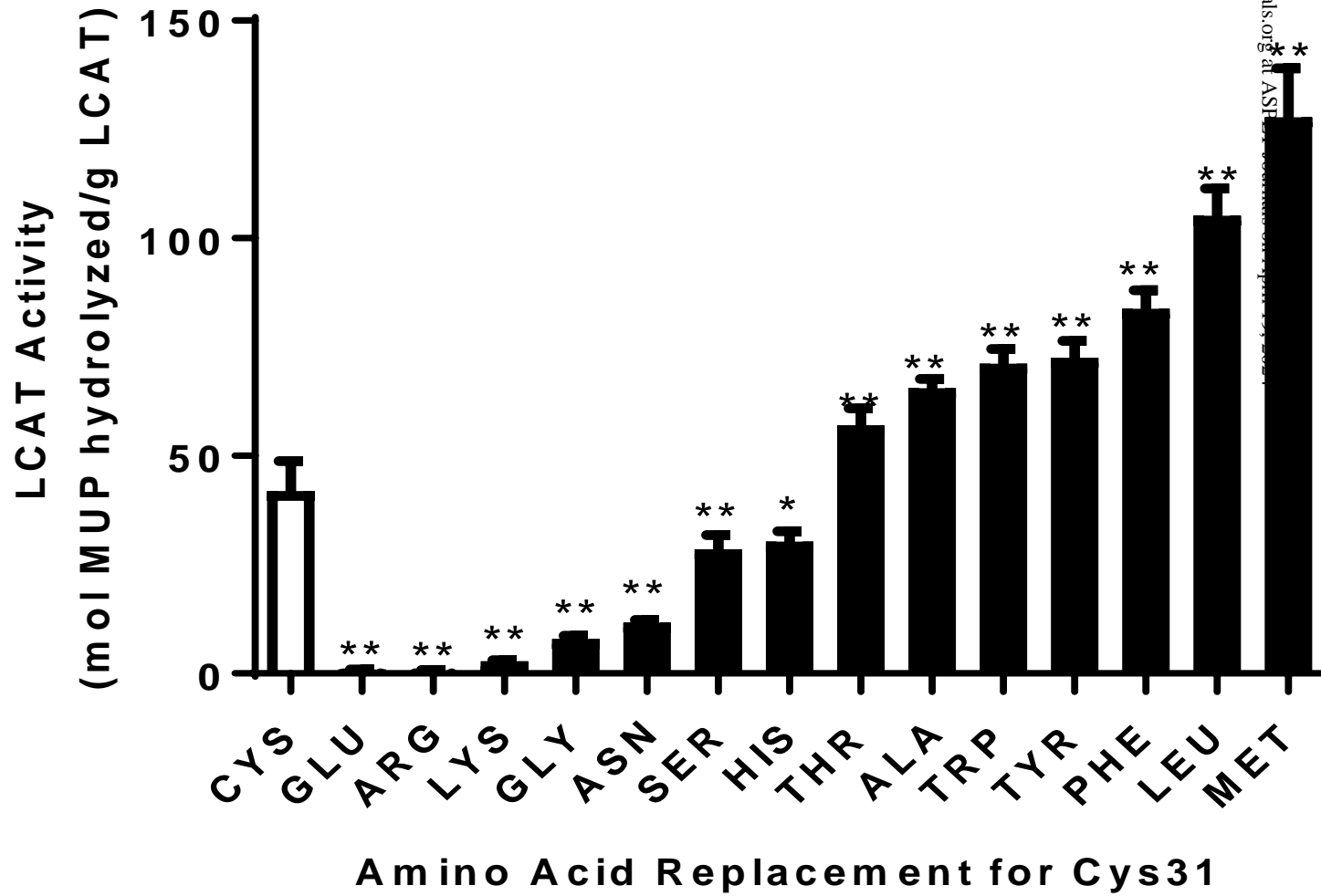
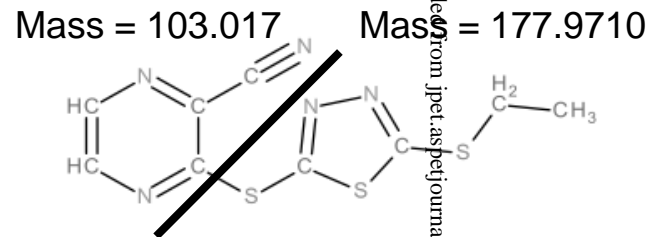
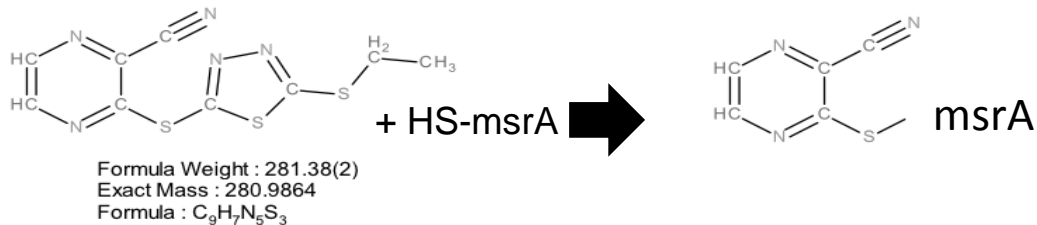


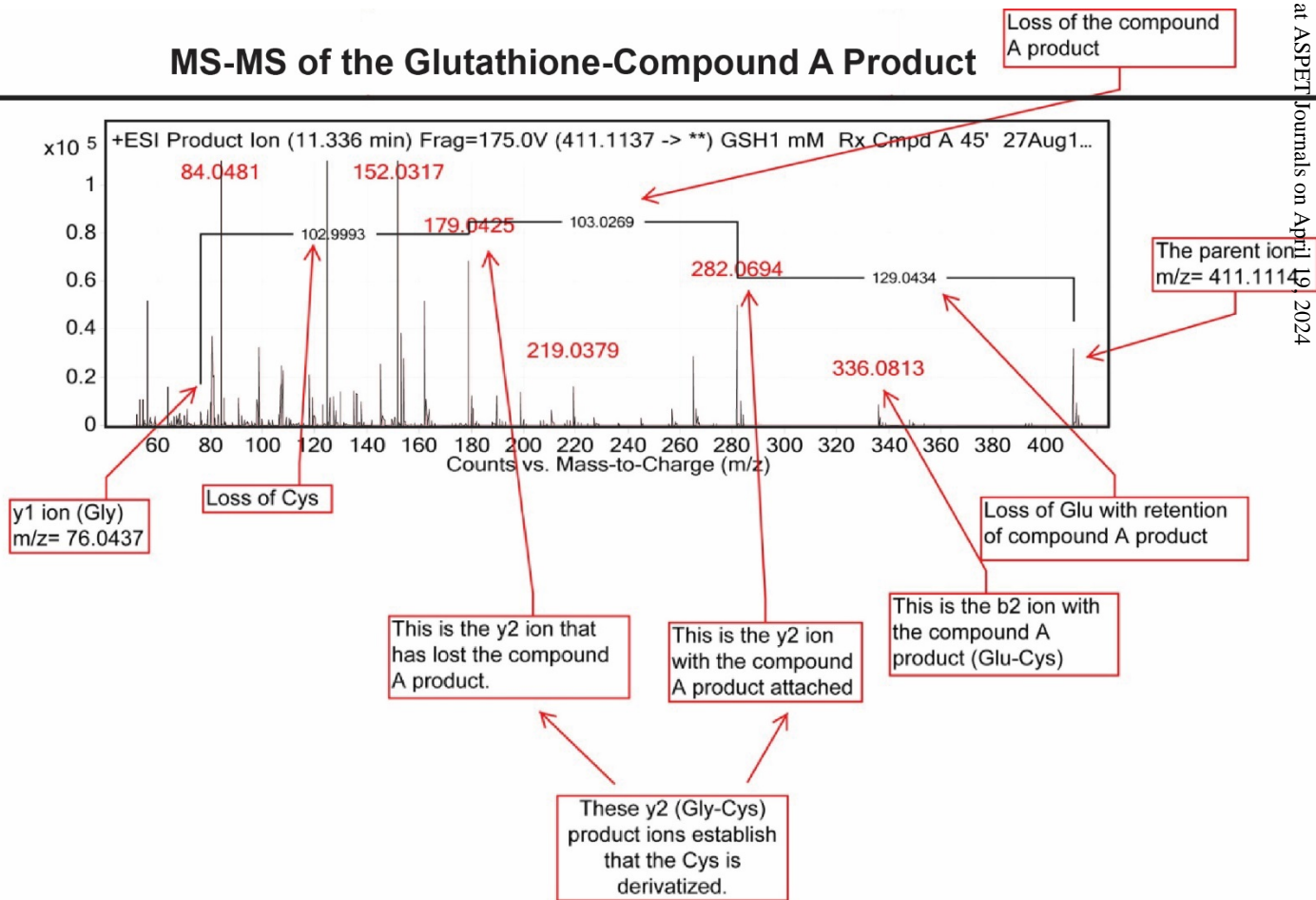
Figure 5

A

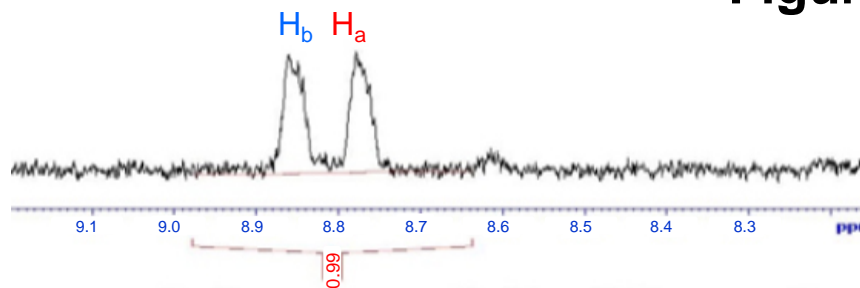


B

MS-MS of the Glutathione-Compound A Product

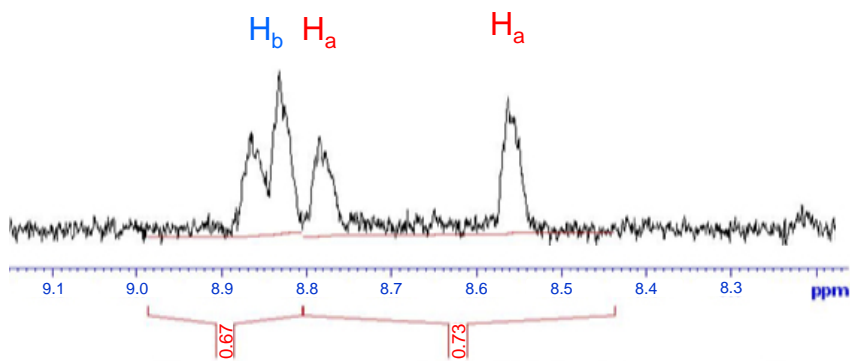


Compound 5 (t = 0)



Compound 5 + Glutathione (mid-reaction)

Cmpd 5 **Cmpd 5 – Glutathione Adduct**



Compound 5 + Glutathione (end of reaction)

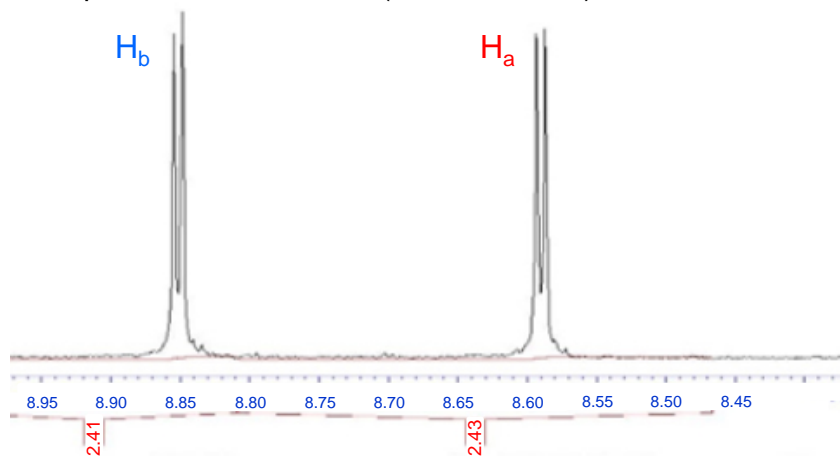
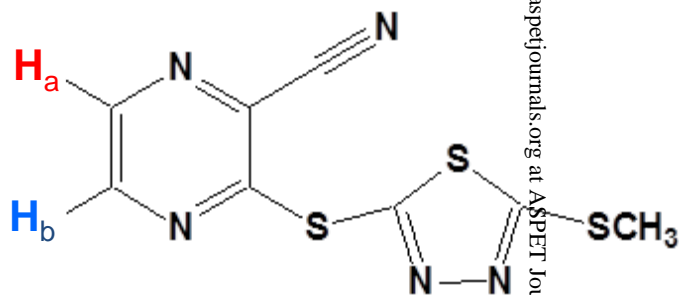


Figure 6A

Compound 5



Compound 5-Glutathione Adduct

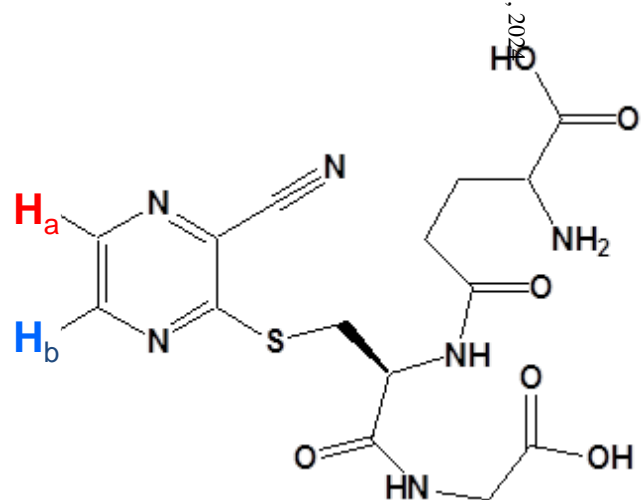


Figure 6B

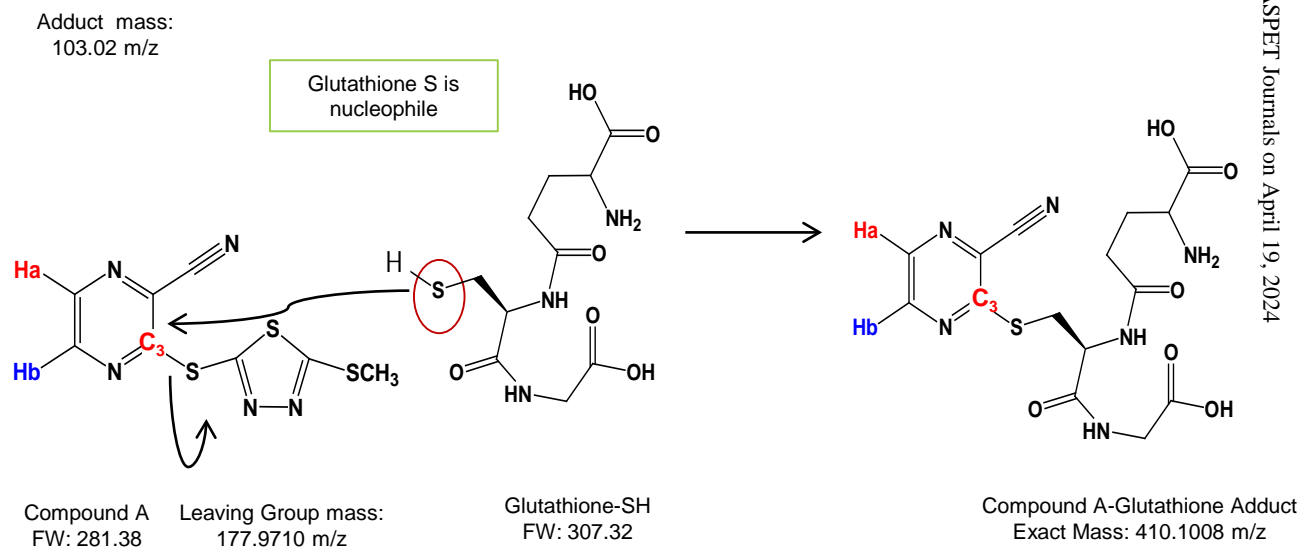
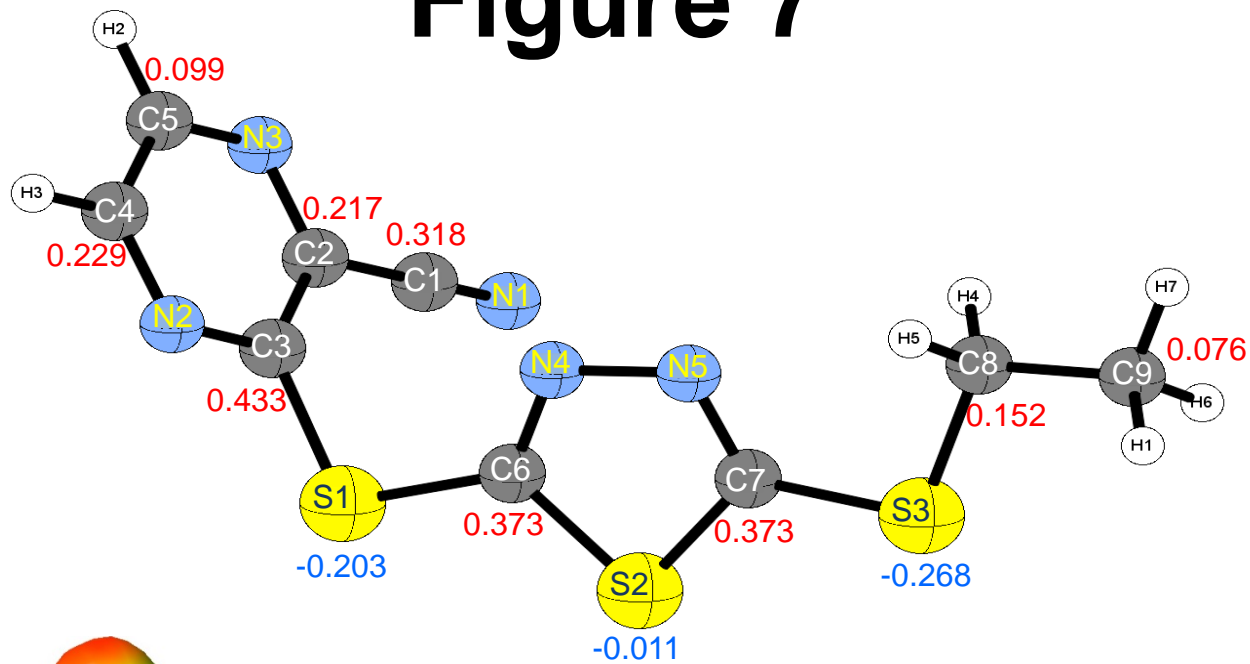


Figure 7

A



B

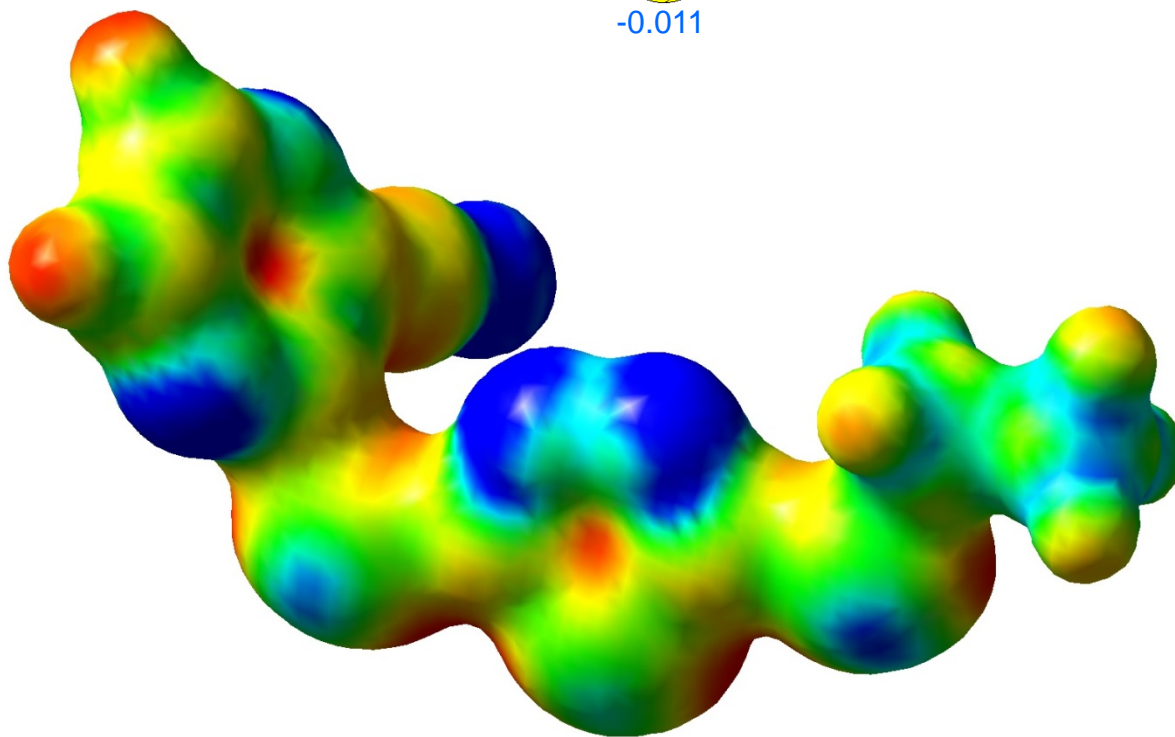
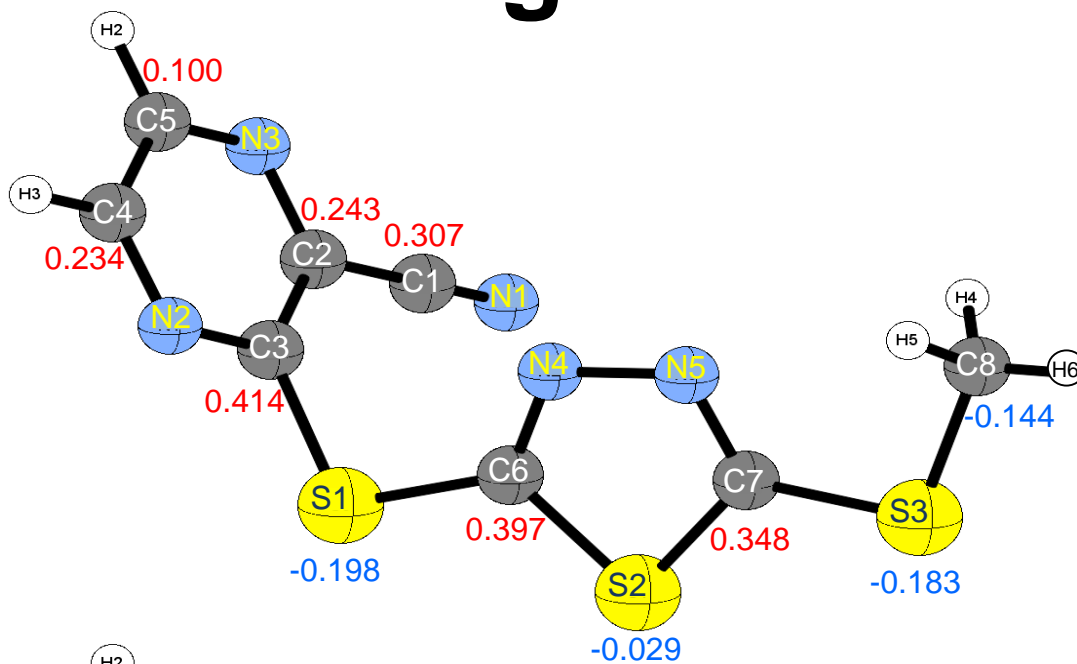


Figure 7

C



D

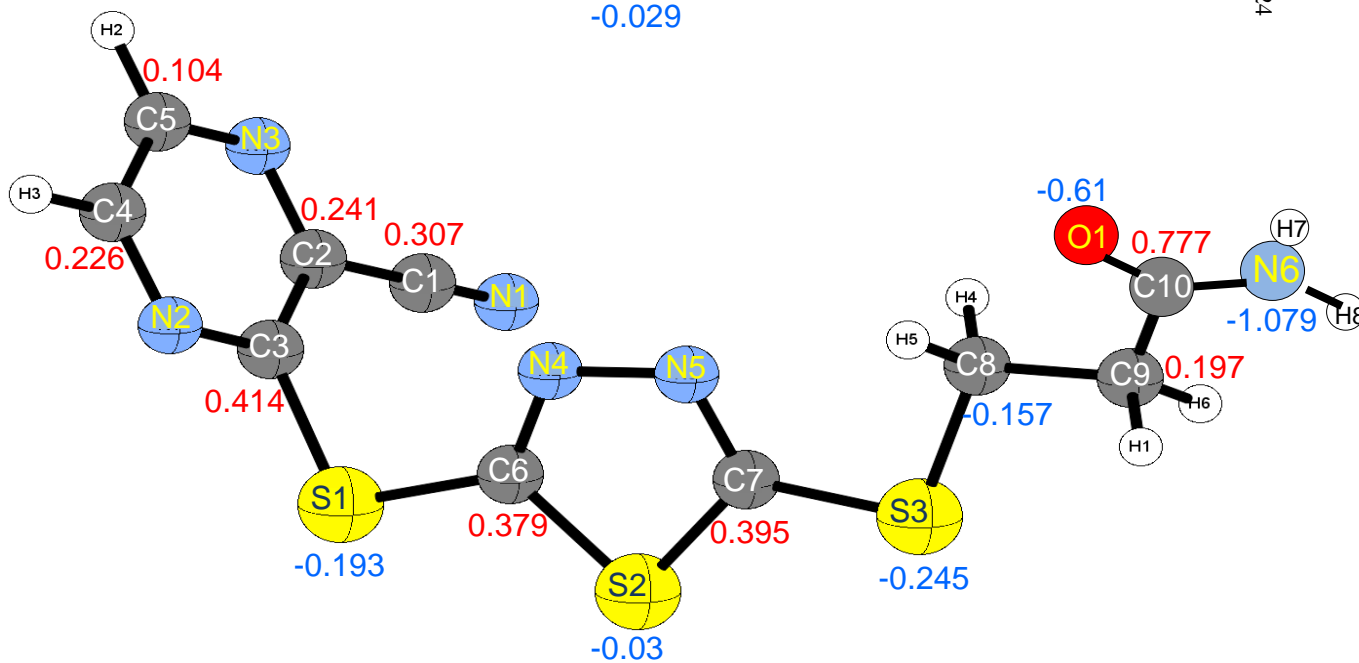
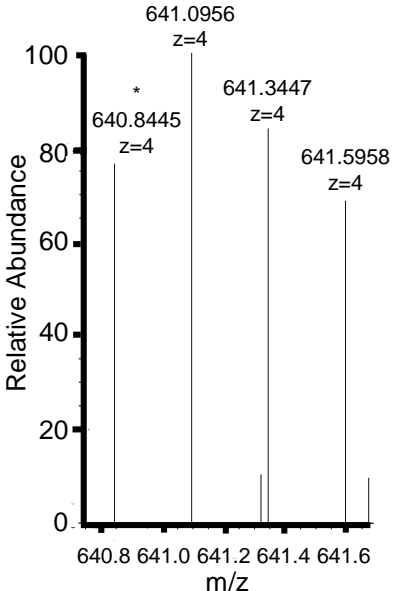


Figure 8

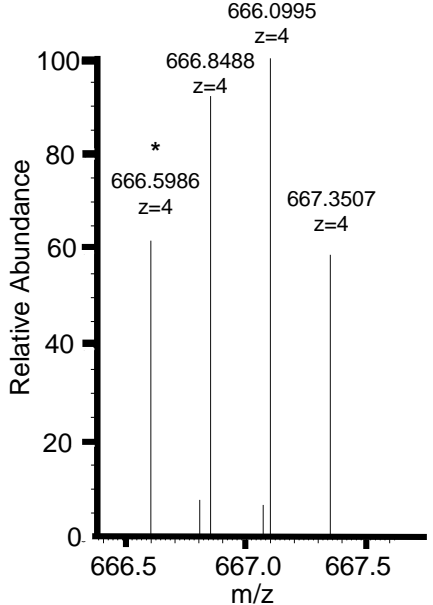
LCAT

A)



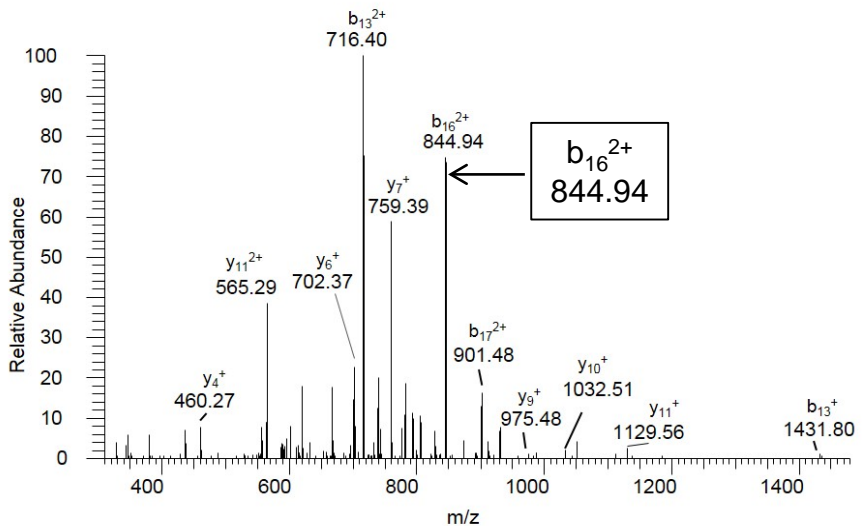
LCAT + Compound A

B)



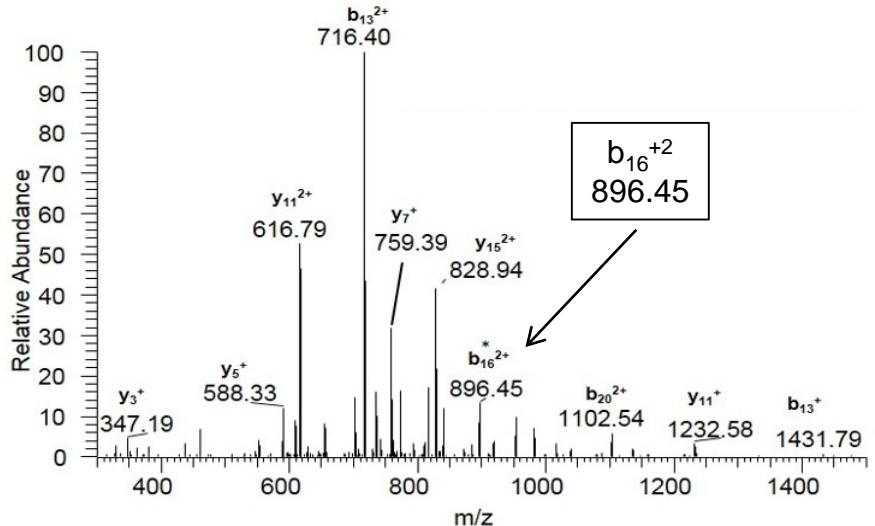
C)

A E L S n J H I T R P V I L V P G C L G N Q L E A J K



D)

A E L S n J H I T R P V I L V P G C L G N Q L E A J K



Downloaded from jpet.aspetjournals.org at ASPET Journals on April 19, 2024

Figure 9

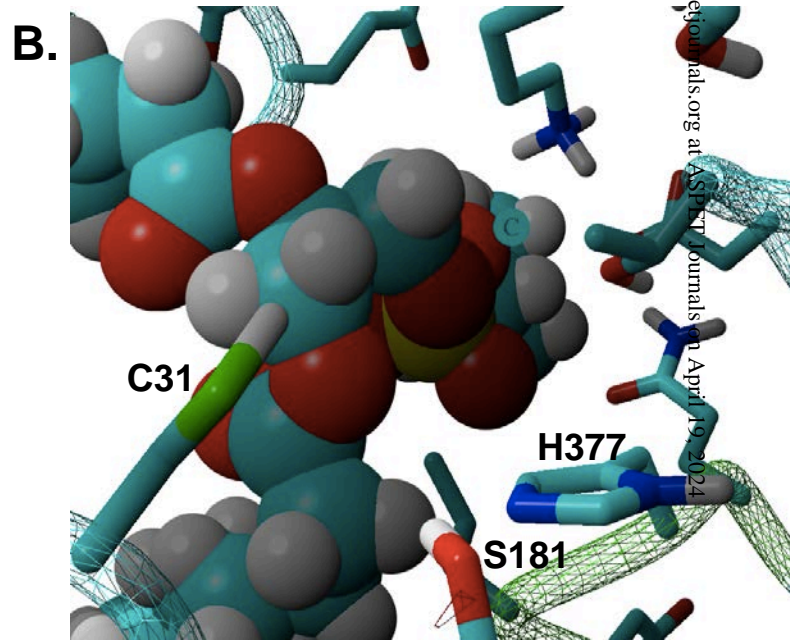
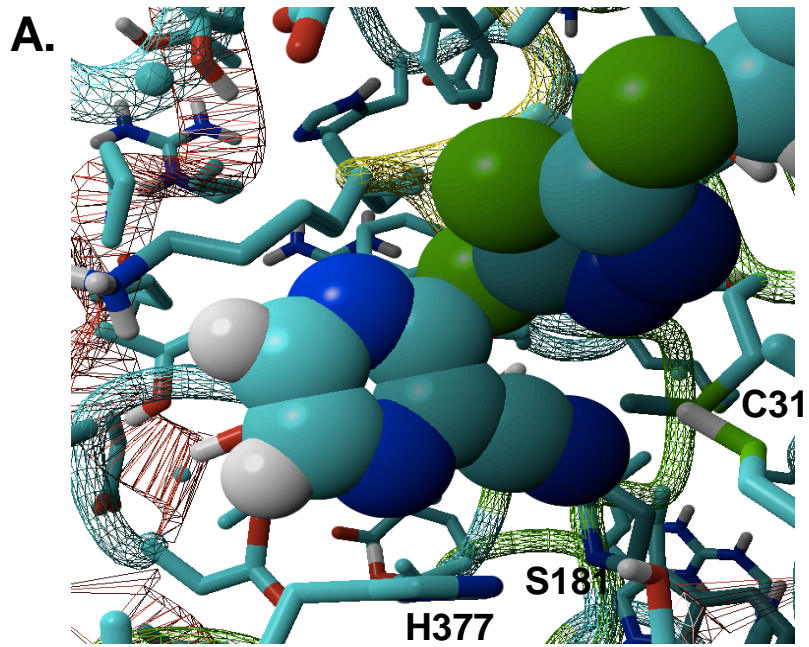
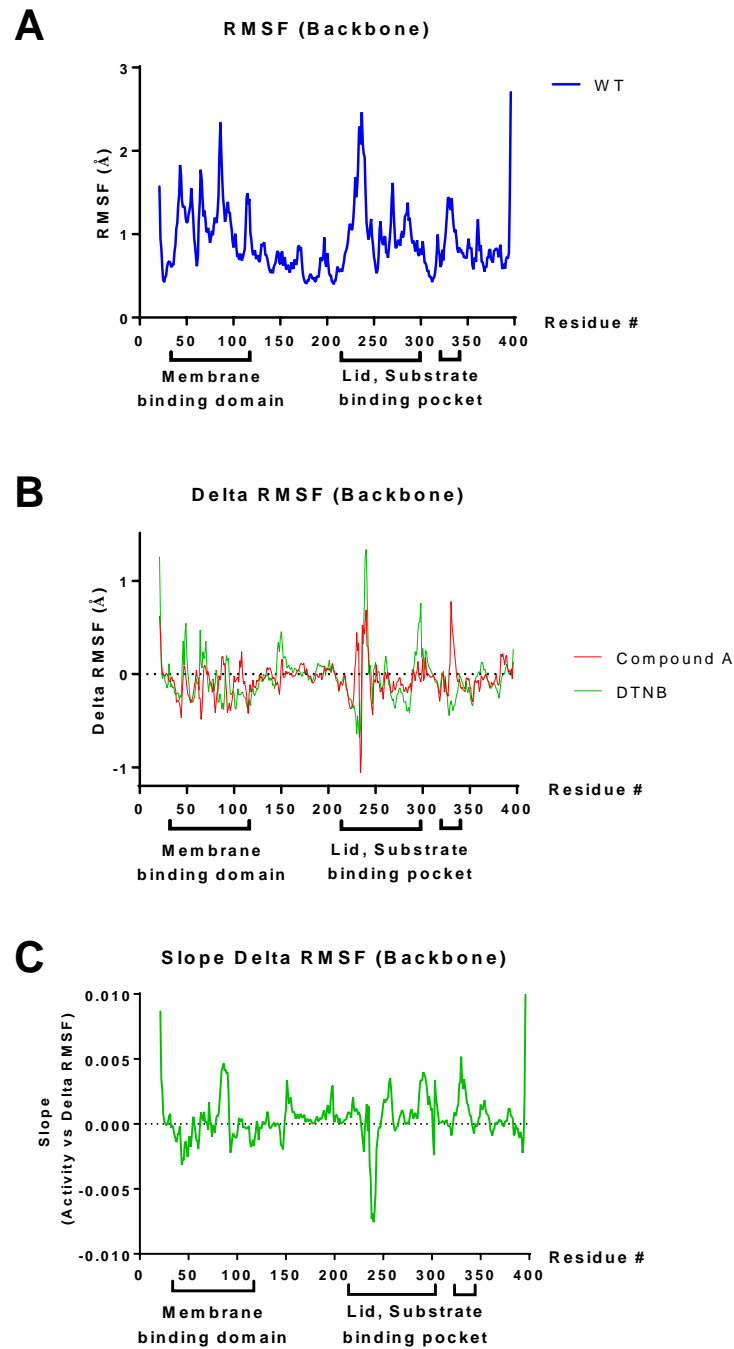


Figure 10



SUPPLEMENTAL MATERIAL

Lecithin:Cholesterol Acyltransferase Activation by Sulfhydryl-Reactive Small Molecules: Role of Cysteine-31

Lita A. Freeman, Stephen J. Demosky Jr., Monika Konaklieva, Rostislav Kuskovsky, Angel Aponte, Alice F. Ossoli, Scott M. Gordon, Ross F. Koby, Kelly A. Manthei, Min Shen, Boris L. Vaisman, Robert D. Shamburek, Ajit Jadhav, Laura Calabresi, Marjan Gucek, John J.G. Tesmer, Rodney L. Levine, Alan T. Remaley

The Journal of Pharmacology and Experimental Therapeutics (JPET)

Chemistry

General procedure for synthesis of derivatives of compound A and β -lactams containing aromatic thiols

All reagents needed for the synthesis of compound A and its derivatives and the β -lactams were purchased from Sigma-Aldrich Chemical Company and used without further purification. Solvents were obtained from Fisher Scientific Company. Thin layer chromatography (TLC) was carried out using EM Reagent plates with a fluorescence indicator (SiO₂-60, F-254). Products were purified by flash chromatography using J.T. Baker flash chromatography silica gel (40 mm).

All compounds were characterized by ¹H and ¹³C NMR spectra (25 °C). Spectra were obtained at 400 MHz for ¹H NMR and 125 MHz for ¹³C NMR in CDCl₃ (Bruker 400 spectrometer, Billerica, MA). Chemical shifts were reported in ppm (δ) relative to the residual solvent peak in the corresponding spectra; chloroform δ 7.26 and δ 77.23. Coupling constants (J) are reported in hertz (Hz). Abbreviations used follow: s = singlet, br = broad singlet, d = doublet, dd = double of doublet, bd = broad doublet, ddd = doublet of doublet of doublet, t = triplet, dt – doublet of triplet, q = quartet, p = pentet, m = multiplet. In most cases, signals due to exchangeable protons were

omitted. ^{13}C NMR spectra were proton broad-band decoupled, but not fluorine broad-band decoupled, and therefore some signals in the spectra are split by $J_{\text{C-F}}$ -coupling.

Derivatives of compound A

Compounds **5-10** (Supplemental Figure 6A, Scheme 1), **12-15** (Supplemental Figure 6B, Scheme 2), and **17, 18** (Supplemental Figure 6C, Scheme 3) were prepared by a modified procedure as reported by Kayser F. *et al.* (ref 1) and Chen Z. *et al.* (ref. 2). To a solution of the corresponding thiol, or phenol **4** (0.85 g, 5.0 mmol) in 15 ml DMF (N, N-Dimethylformamide) 3-chloropyrazine-2-carbonitrile (0.66 g, 4.76 mmol) and Na_2CO_3 (1.01 g, 9.52 mmol), or substituted chloropyridines, or chlorobenzenes, were added respectively and the resulting mixture was refluxed at 80 °C for 12 h. The DMF was evaporated at reduced pressure and the compound A residue was recrystallized from ethyl acetate. The rest of the compounds were purified by flash chromatography on silica gel with ethyl acetate:hexanes (5-100% gradient).

NMR spectra of Compound A derivatives

Compound 5 (3-((5-(methylthio)-1,3,4-thiadiazol-2-yl)thio)pyrazine-2-carbonitrile) (**5**)

The product was purified by recrystallization from ethyl acetate to give light yellow crystals (65% ^1H NMR (400 MHz, CDCl_3): δ 8.57 (1H, d, $J = 2.0$), 8.35 (1H, d, $J = 2.0$), 3.05 (3H, s).

Compound 6 3-(Thiophen-2-ylsulfanyl)-pyrazine-2-carbonitrile (**6**)

The product was purified by flash chromatography from ethyl acetate/hexanes (0 – 25%) to give light yellow crystals (65% ^1H NMR (400 MHz, CDCl_3): δ 8.45 (1H, d, $J = 2.0$), 8.53 (1H, d, $J = 2.0$), 7.62 (1H, d $J = 4.13$), 7.00 (1H, d, $J = 4.13$), 2.5 (3H, s).

Compound 7 3-(4-Methylsulfanyl-phenylsulfanyl)-pyrazine-2-carbonitrile (**7**)

The product was purified by flash chromatography from ethyl acetate/hexanes (0 – 25%) to give light yellow crystals (75% ^1H NMR (400 MHz, CDCl_3): δ 8.57 (1H, d, $J = 2.15$), 7.96 (1H, d, $J = 2.15$), 7.52 (2H, dd, $J = 8.10, 2.01$), 7.50 (2H, dd, $J = 8.10, 2.01$), 2.45 (3H, s).

Compound 8 3-(4-Nitro-phenoxy)-pyrazine-2-carbonitrile (**8**)

The product was purified by flash chromatography from ethyl acetate/hexanes (0 – 25%) to give bright yellow crystals (55% ¹H NMR (400 MHz, CDCl₃): δ 8.93 (1H, d, *J* = 3.40), 8.23 (1H, dd, *J* = 9.40, 2.81), 8.16 (1H, d, *J* = 3.40), 7.66 (2H, dd, *J* = 9.40, 3.09).

Compound 10 3-[5-(3-Cyano-pyrazin-2-ylsulfanyl)-[1,3,4]thiadiazol-2-ylsulfanyl]-propionamide (10)

The product was purified by flash chromatography from ethyl acetate/hexanes (0 – 25%) to give light yellow crystals (75% ¹H NMR (400 MHz, CDCl₃): δ 8.58 (1H, d, *J* = 2.15), 8.53 (1H, d, *J* = 2.15), 2.90 (2H, dt, *J* = 7.03, 2.83), 2.51 (2H, dt, *J* = 7.03, 1.33).

Compound 12 2-(5-Methylsulfanyl-[1,3,4]thiadiazol-2-ylsulfanyl)-3-trifluoromethyl-pyridine (12)

The product was purified by flash chromatography from ethyl acetate/hexanes (0 – 25%) to give light yellow crystals (55% ¹H NMR (400 MHz, CDCl₃): δ 8.67 (1H, dd, *J* = 4.75, 1.50), 8.20 (1H, dd, *J* = 7.83, 4.75), 7.33 (1H, dd, *J* = 7.83, 1.50, *J*_{C-F} = 1.08), 3.05 (3H, s).

Compound 13 2-(5-Methylsulfanyl-[1,3,4]thiadiazol-2-ylsulfanyl)-3-nitro-pyridine (13)

The product was purified by flash chromatography from ethyl acetate/hexanes (0 – 25%) to give yellow crystals (75% ¹H NMR (400 MHz, CDCl₃): δ 8.80 (1H, dd, *J* = 4.83, 1.91), 8.11 (1H, dd, *J* = 7.41, 1.91), 7.47 (1H, dd, *J* = 7.41, 4.83), 3.05 (3H, s).

Compound 14 3-Nitro-2-(4-nitro-phenylsulfanyl)-pyridine (14)

The product was purified by flash chromatography from ethyl acetate/hexanes (0 – 25%) to give bright yellow crystals (60% ¹H NMR (400 MHz, CDCl₃): δ 8.71 (1H, dd, *J* = 4.83, 1.91), 8.34 (1H, dd, *J* = 8.40, 2.01), 8.02 (1H, dd, *J* = 7.41, 1.91), 7.85 (2H, dd, *J* = 8.40, 3.09) 7.47 (2H, dd, *J* = 7.41, 4.83).

Compound 15 6-(4-Nitro-phenylsulfanyl)-nicotinonitrile (15)

The product was purified by flash chromatography from ethyl acetate/hexanes (0 – 25%) to give yellow crystals (55% ¹H NMR (400 MHz, CDCl₃): δ 9.02 (1H, dd, *J* = 2.10, 0.81), 8.30 (2H, dd, *J* = 8.40, 2.01), 8.10 (1H, dd, *J* = 7.50, 2.10), 7.84 (2H, dd, *J* = 8.40, 3.09), 7.02 (1H, dd, *J* = 7.50, 0.81).

Compound 17 2-Nitro-1(4-methylsulfanyl-phenylsulfanyl)-benzene (17)

The product was purified by flash chromatography from ethyl acetate/hexanes (0 – 25%) to give yellow crystals (60% ¹H NMR (400 MHz, CDCl₃): δ 8.18 (1H, dd, *J* = 7.80, 1.42), 8.08 (1H, ddd, *J* = 7.80, 7.41, 1.42), 7.85 (1H, dd, *J* = 7.41, 1.42), 7.57 (1H, ddd, *J* = 7.80, 7.47, 1.42) 7.45 (2H, dd, *J* = 8.10, 2.01), 6.98 (2H, dd, *J* = 8.10, 2.01), 2.45 (3H, s).

Compound 18 2-Nitro-(4-trifluoromethyl)-1-(4-methylsulfanyl-phenylsulfanyl)-benzene (**18**)

The product was purified by flash chromatography from ethyl acetate/hexanes (0 – 25%) to give yellow crystals (50% ¹H NMR (400 MHz, CDCl₃): δ 8.97 (1H, d, *J* = 1.49), 8.61 (1H, d, *J* = 1.49), 7.55 (2H, dd, *J* = 8.10, 2.01), 7.22 (2H, dd, *J* = 8.10, 2.01), 2.47 (3H, s).

***β*-Lactams**

β-Lactams **19** and **20** (Table 1; Supplemental Figure 6D, Scheme 4) were prepared from the commercially available aldehydes as described earlier (ref 3, 4), and their cis-relative stereochemistry confirmed by NMR (ref. 5).

References

1. Kayser F, LaBelle M, Shan B, Zhang J, and Zhou M (2008) Methods for treating atherosclerosis. US Patent #8426358 (United States: Amgen, Inc).
2. Chen Z, Wang SP, Krsmanovic ML, Castro-Perez J, Gagen K, Mendoza V, Rosa R, Shah V, He T, Stout SJ, Geoghagen NS, Lee SH, McLaren DG, Wang L, Roddy TP, Plump AS, Hubbard BK, Sinz CJ, Johns DG. Small molecule activation of lecithin cholesterol acyltransferase modulates lipoprotein metabolism in mice and hamsters. *Metabolism*. 2012;61:470-481
3. Turos E, Konaklieva MI, Ren RXF, Shi H, Gonzalez, Dickey S, Lim D. N-Thiolated Bicyclic and Monocyclic Beta-Lactams. *Tetrahedron*. 2000; 56:5571-5578.
4. Long TE, Turos E, Konaklieva MI, Blum AL, Amry A, Baker EA, Suwandi LS, McCain MD, Rahman MF, Dickey S, Lim D. V. Effect of Aryl Ring Fluorination on the Antibacterial Properties of C4 Aryl-Substituted N-Methylthio *β*-Lactams. *Bioorganic & Medicinal Chemistry*. 2003;11:1859-1863.
5. cis-Disubstituted *β*-lactams typically display a coupling constant of 4.8–6.0 Hz for the two vicinal protons on the ring; for the trans isomer, the value is normally in the range of 1–3 Hz.

Supplemental Table S1:

Primer Sequences – Cys31 to:

Ala **Forward** CTG-GTG-CCT-GGC-**GCC**-CTG-GGC-AAT-CAG

Ala **Reverse** CTG-ATT-GCC-CAG-**GGC**-GCC-AGG-CAC-CAG

Arg **Forward** CTG-GTG-CCT-GGC-**CGC**-CTG-GGC-AAT-CAG

Arg **Reverse** CTG-ATT-GCC-CAG-**GCG**-GCC-AGG-CAC-CAG

Asn **Forward** CTG-GTG-CCT-GGC-**AAC**-CTG-GGC-AAT-CAG

Asn **Reverse** CTG-ATT-GCC-CAG-**GTT**-GCC-AGG-CAC-CAG

Glu **Forward** CTG-GTG-CCT-GGC-**GAA**-CTG-GGC-AAT-CAG

Glu **Reverse** CTG-ATT-GCC-CAG-**TTC**-GCC-AGG-CAC-CAG

Gly **Forward** CTG-GTG-CCT-GGC-**GGA**-CTG-GGC-AAT-CAG

Gly **Reverse** CTG-ATT-GCC-CAG-**TCC**-GCC-AGG-CAC-CAG

His **Forward** CTG-GTG-CCT-GGC-**CAC**-CTG-GGC-AAT-CAG

His **Reverse** CTG-ATT-GCC-CAG-**GTG**-GCC-AGG-CAC-CAG

Leu **Forward** CTG-GTG-CCT-GGC-**CTC**-CTG-GGC-AAT-CAG

Leu **Reverse** CTG-ATT-GCC-CAG-**GAG**-GCC-AGG-CAC-CAG

Lys **Forward** CTG-GTG-CCT-GGC-**AAA**-CTG-GGC-AAT-CAG

Lys **Reverse** CTG-ATT-GCC-CAG-**TTT**-GCC-AGG-CAC-CAG

Met **Forward** CTG-GTG-CCT-GGC-**ATG**-CTG-GGC-AAT-CAG

Met **Reverse** CTG-ATT-GCC-CAG-**CAT**-GCC-AGG-CAC-CAG

Phe **Forward** CTG-GTG-CCT-GGC-**TTC**-CTG-GGC-AAT-CAG

Phe **Reverse** CTG-ATT-GCC-CAG-**GAA**-GCC-AGG-CAC-CAG

Ser **Forward** CTG-GTG-CCT-GGC-**AGC**-CTG-GGC-AAT-CAG

Ser **Reverse** CTG-ATT-GCC-CAG-**GCT**-GCC-AGG-CAC-CAG

Thr **Forward** CTG-GTG-CCT-GGC-**ACC**-CTG-GGC-AAT-CAG

Thr **Reverse** CTG-ATT-GCC-CAG-**GGT**-GCC-AGG-CAC-CAG

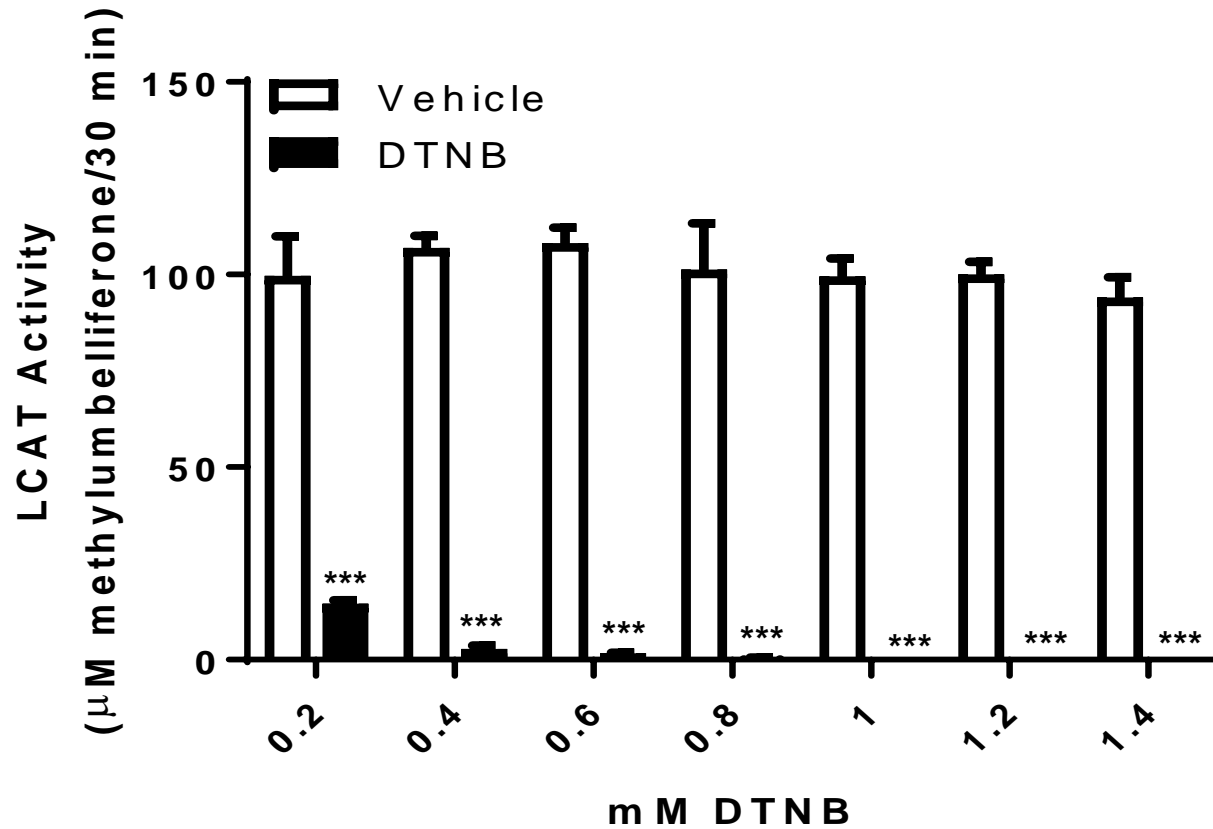
Trp **Forward** CTG-GTG-CCT-GGC-**TGG**-CTG-GGC-AAT-CAG

Trp **Reverse** CTG-ATT-GCC-CAG-**CCA**-GCC-AGG-CAC-CAG

Tyr **Forward** CTG-GTG-CCT-GGC-**TAC**-CTG-GGC-AAT-CAG

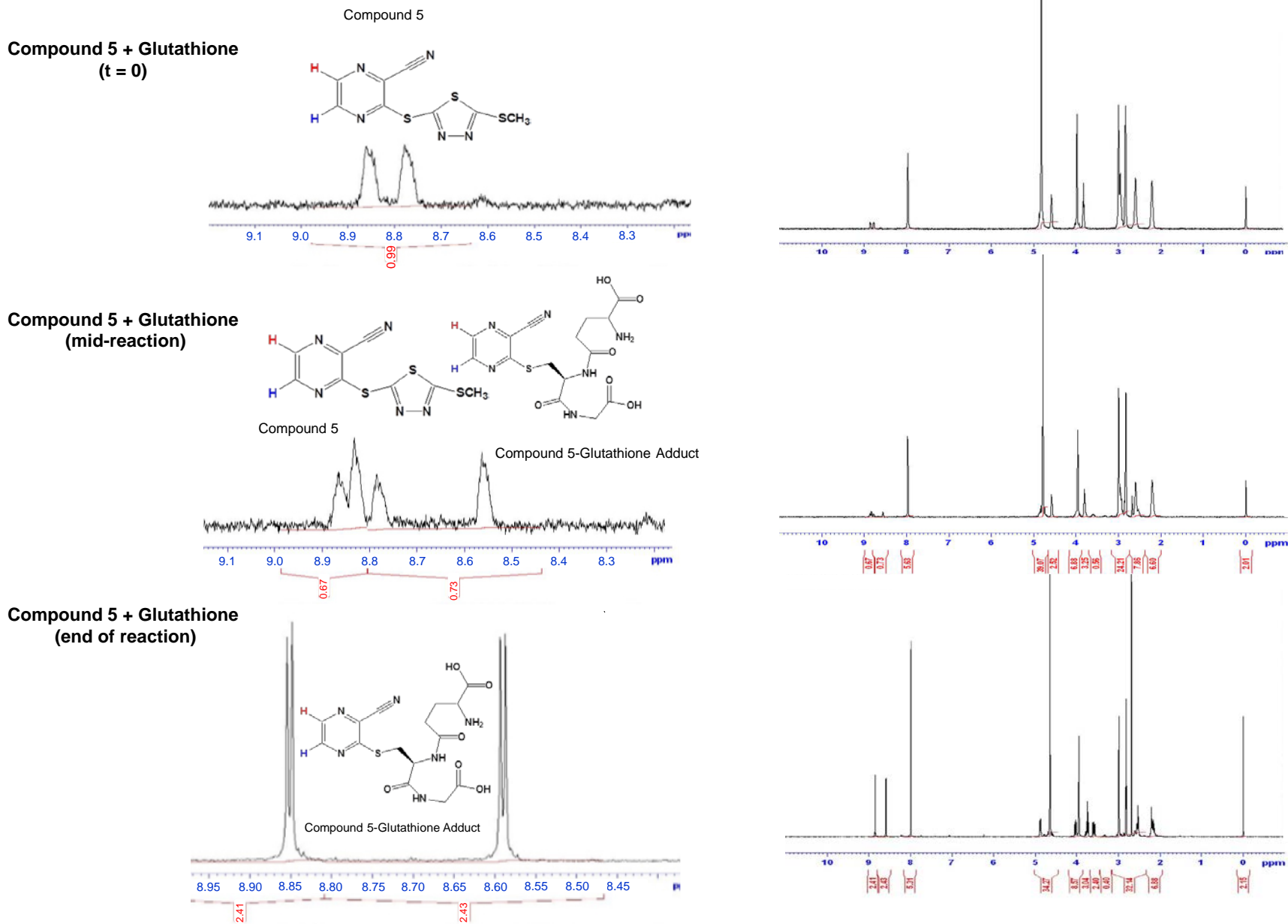
Tyr **Reverse** CTG-ATT-GCC-CAG-**GTA**-GCC-AGG-CAC-CAG

Supplemental Figure 1



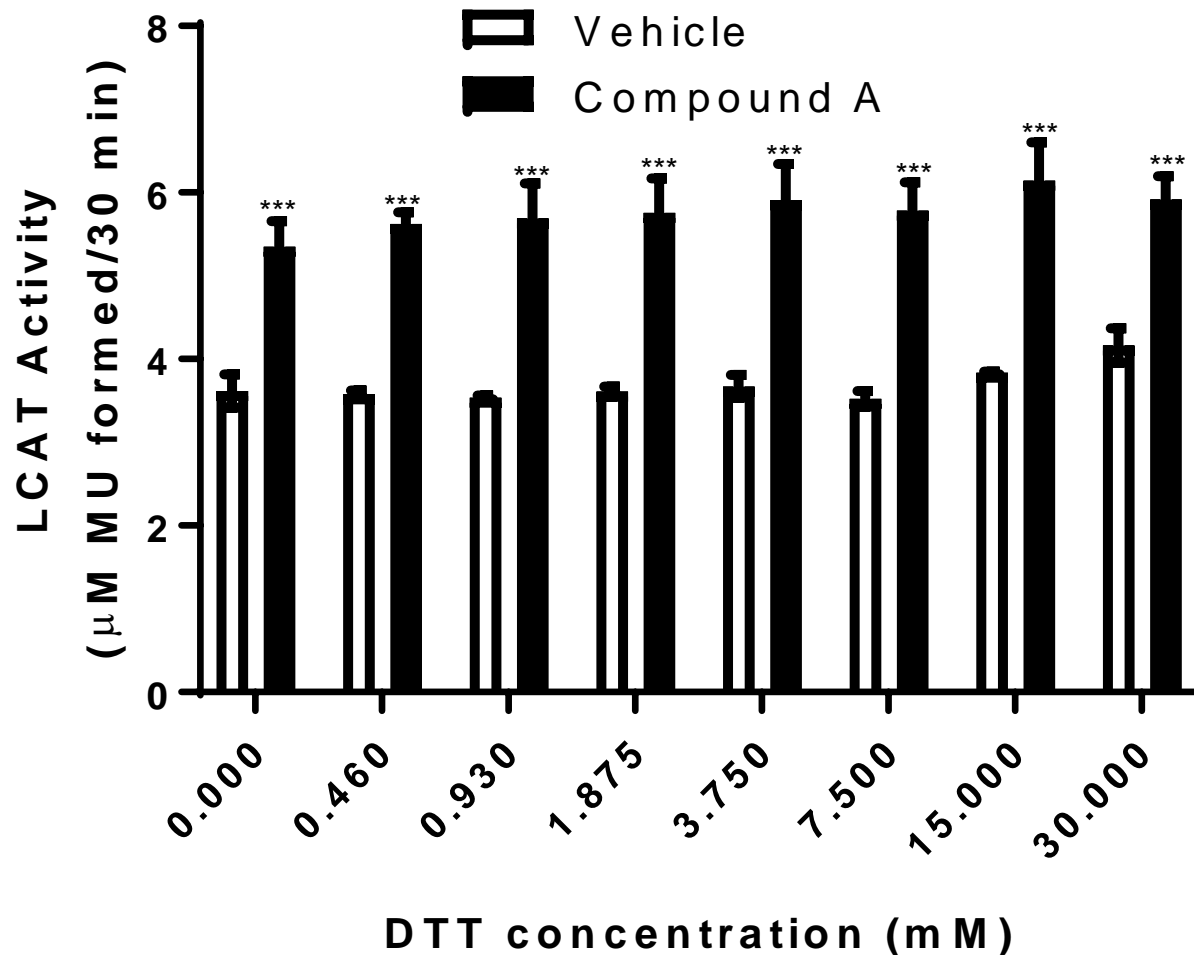
Supplemental Figure 1: DTNB inhibition of LCAT. Recombinant human LCAT was incubated in the presence of the indicated concentration of DTNB (■) or with just vehicle (□) in vitro and LCAT activity was measured using MUP (0.025 mM) as the substrate. Results represent mean \pm SD of at least triplicates. *** ($p < 0.0002$) compared to WT-LCAT treated under the same conditions.

Supplemental Figure 2

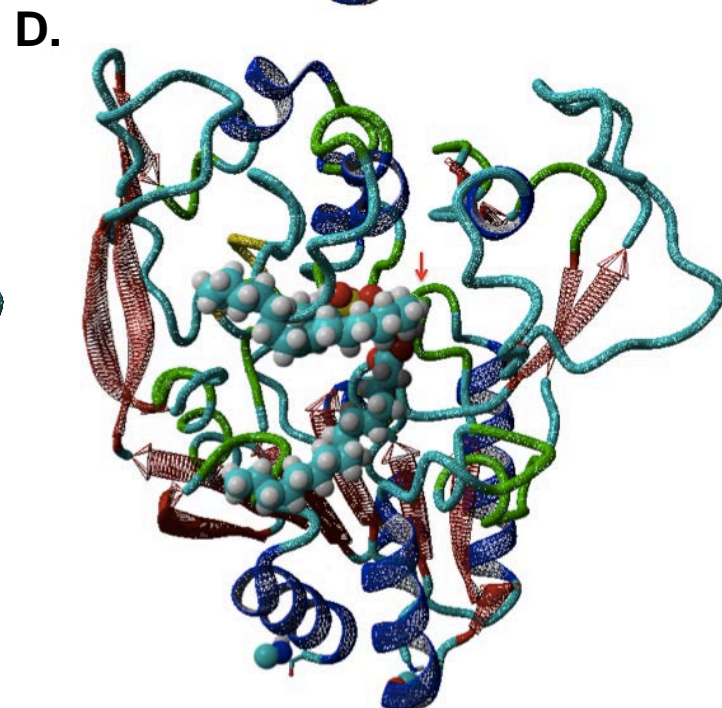
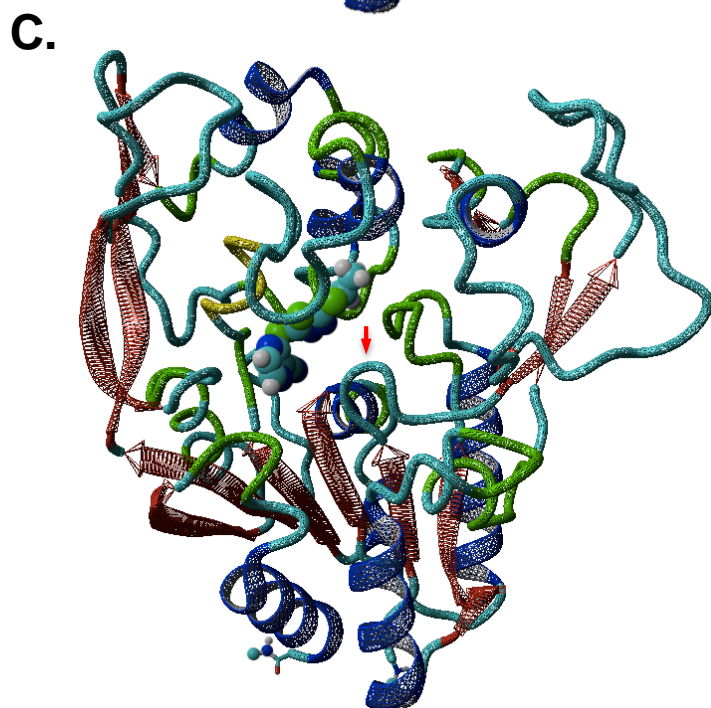
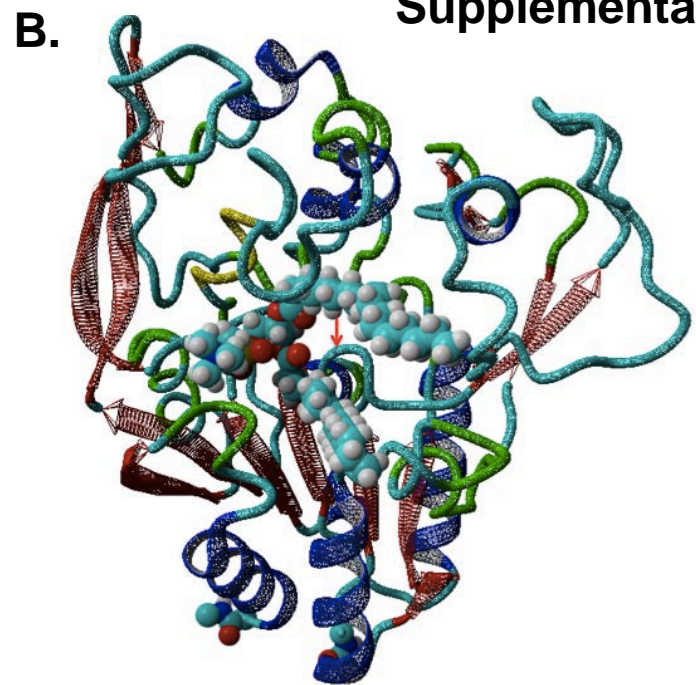
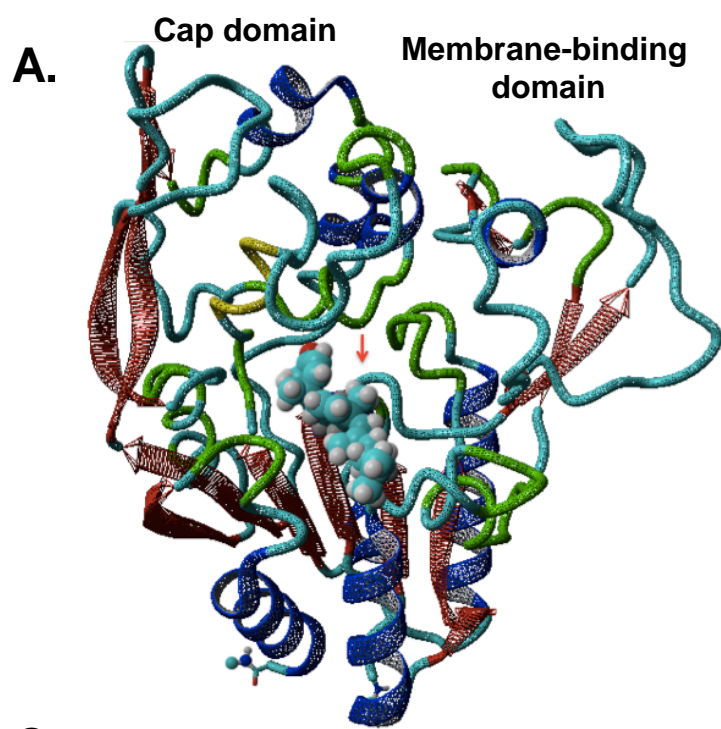


Supplemental Figure 2: NMR analysis of Compound 5-glutathione adduct. (Left) Same as Figure 6A, with structures of Compound 5 and the glutathione-Compound 5 adduct shown over the relevant peaks. (Right) Full NMR spectra for reaction of Compound A with glutathione.

Supplemental Figure 3

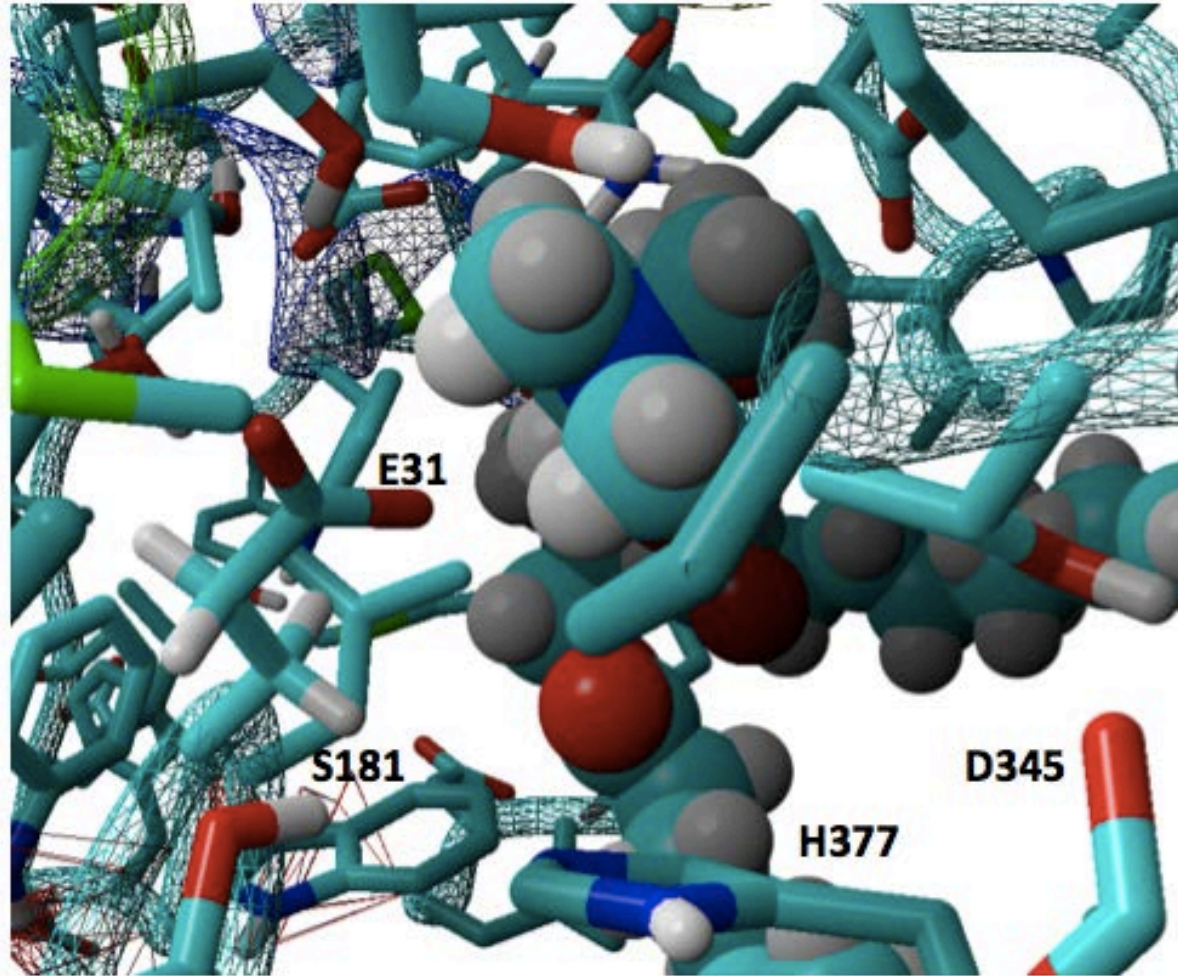


Supplemental Figure 3: DTT does not reverse LCAT activation by Compound A. WT-LCAT was incubated with Compound A (■) or vehicle (□) in the presence of increasing amounts of DTT for 30 min at 37°C and LCAT activity was measured with MUP as the substrate. Results represent mean +/- SD of at least triplicates. *** (p<0.005) compared to vehicle control.



Supplemental Figure 4E

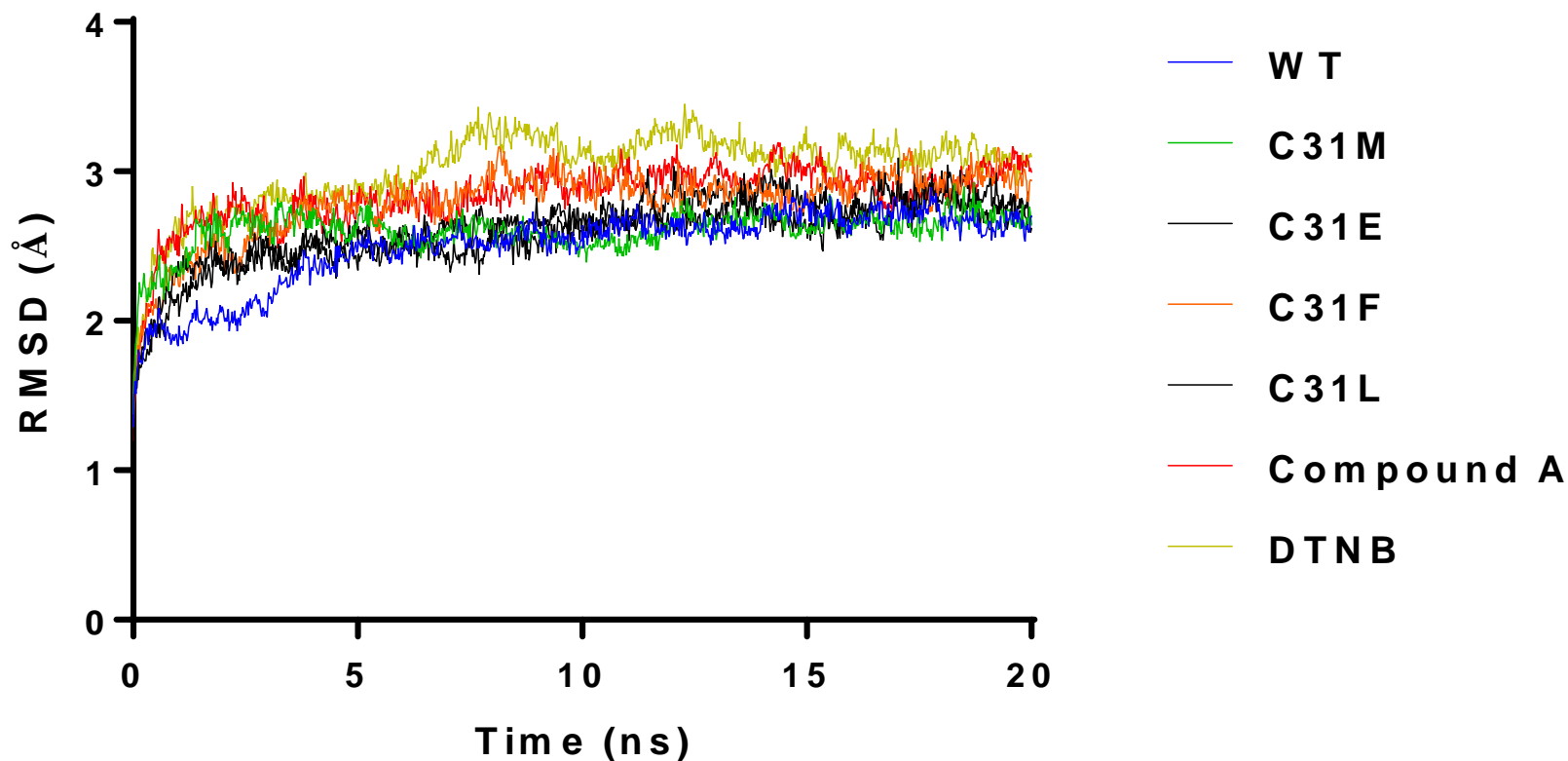
E.



Supplemental Figure 4: Molecular modeling of: (A) WT-LCAT docked with cholesterol in its active site; (B) WT-LCAT docked with POPC in its active site; (C) WT-LCAT docked with Compound A in its active site; (D) LCAT-C31E docked with POPC in its active site; (E) LCAT-C31E (close-up view) docked with POPC in its active site, showing a possible ionic interaction between Glu31 and the positively charged choline head group of phosphatidylcholine. **A, B, C, D:** Red arrow shows location of position 31 (Cys in A B, and C; Glu in D). The cap and membrane-binding domains are shown in panel A.

Supplemental Figure 5

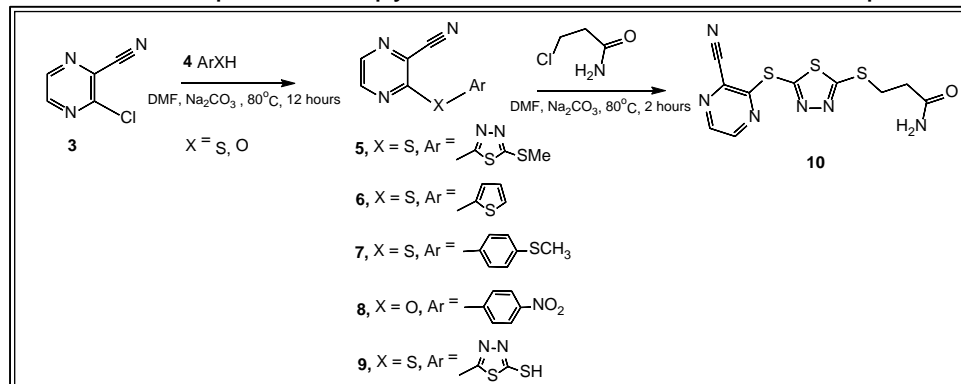
RMSD (Backbone)



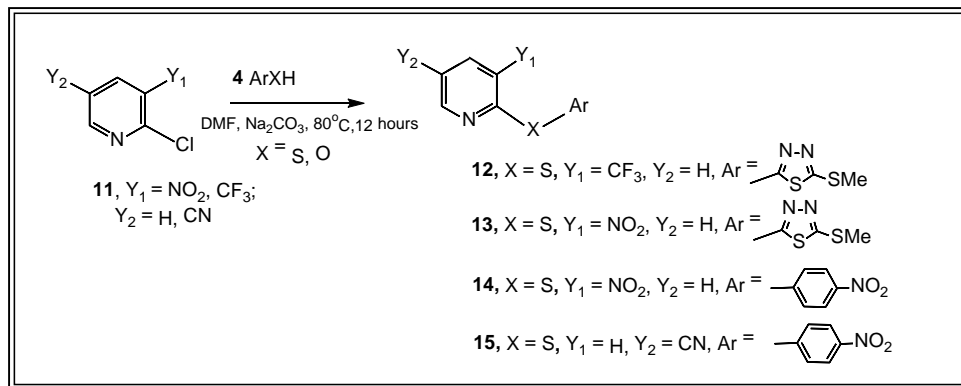
Supplemental Figure 5: Molecular dynamics simulations of LCAT. The overall root-mean-square deviation (RMSD) was determined by all-atom molecular dynamics simulations of LCAT-WT, -C31M, -C31E, -C31F, -C31L, as well as WT-LCAT modified by Compound A and DTNB. Structures reached a stable state after relaxing in water at 37°C for 20 ns.

Supplemental Figure 6A-C

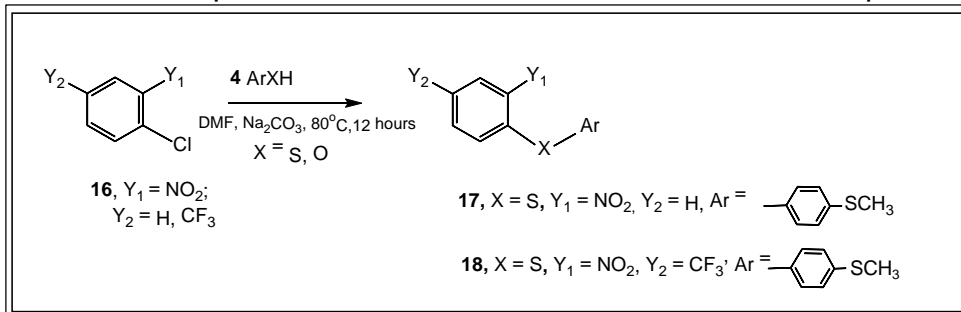
A Scheme 1: Preparation of pyrazine-based derivatives of Compound A.



B Scheme 2: Preparation of pyridine-based derivatives of Compound A.

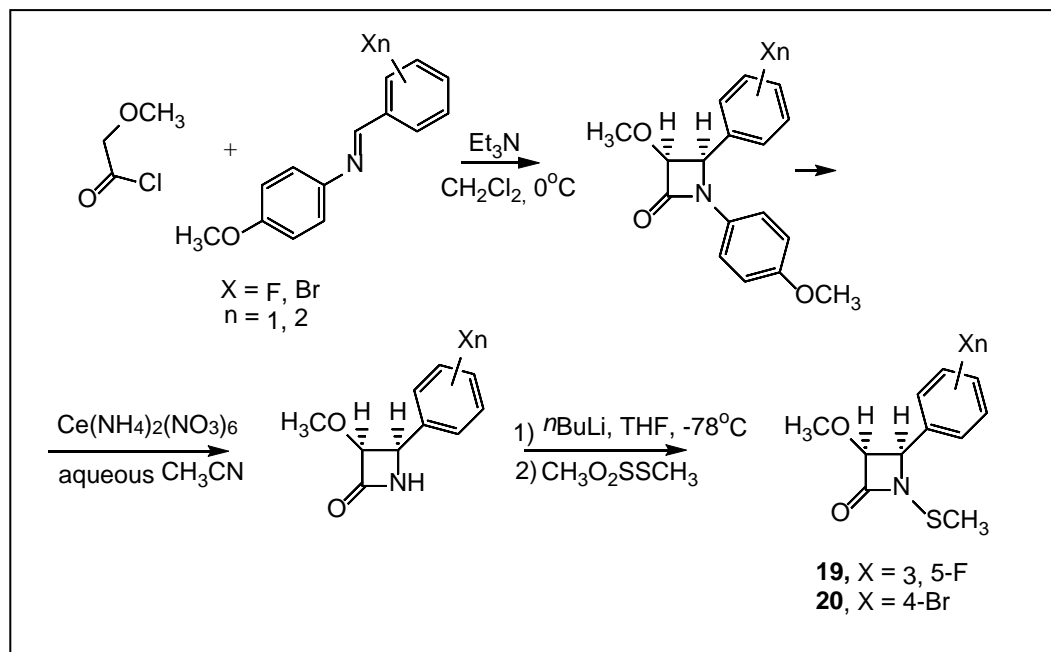


C Scheme 3: Preparation of benzene-based derivatives of Compound A.



Supplemental Figure 6D

Scheme 4. Preparation of Compounds **19** and **20**

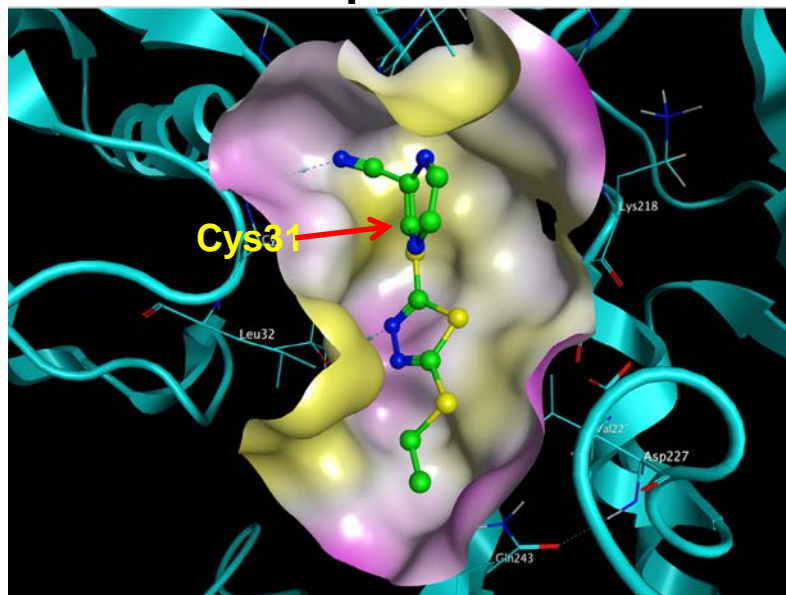


Supplemental Figure 6: Scheme for synthesis of Compound A derivatives. (A) Scheme 1 - Preparation of pyrazine-based derivatives of Compound A. (B) Scheme 2 - Preparation of pyridine-based derivatives of Compound A. (C) Scheme 3 - Preparation of benzene-based derivatives of Compound A. (D) Scheme 4 - Preparation of the N-alkylthio-substituted b-lactams, Compounds **19** and **20**.

Supplemental Figure 7A-D

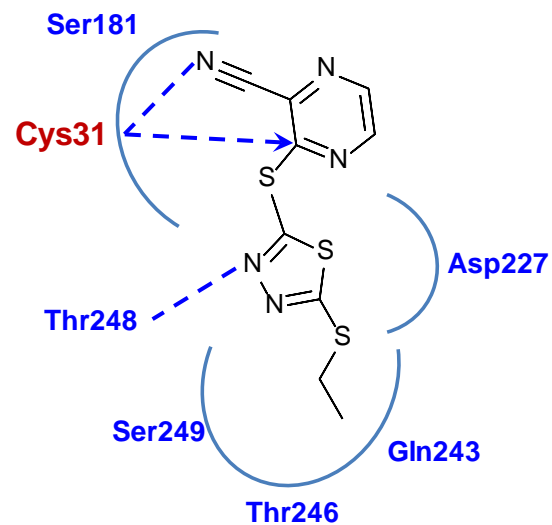
Compound A

A.



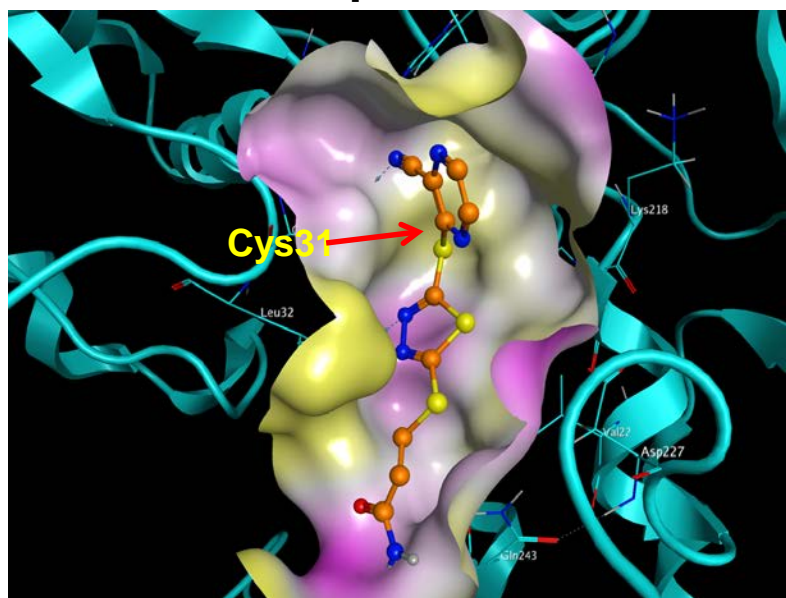
B.

Compound A



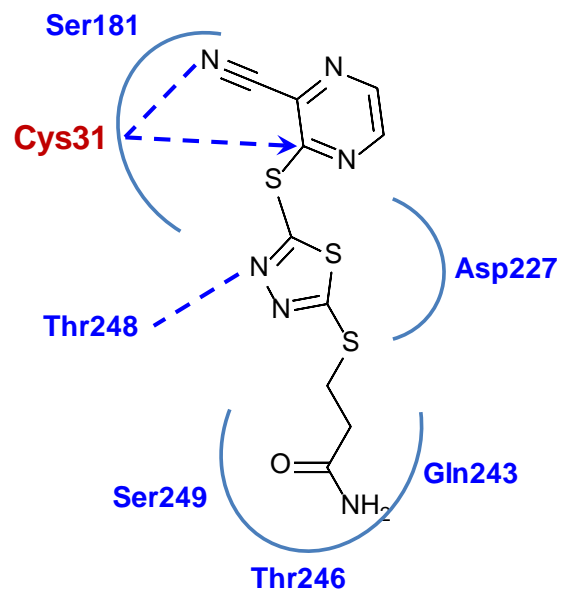
Compound 10

C.



D.

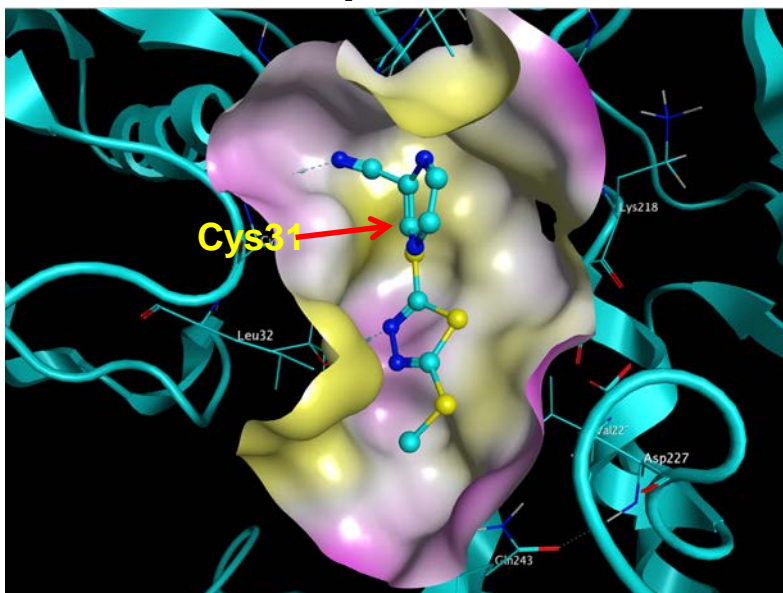
Compound 10



Supplemental Figure 7E,F

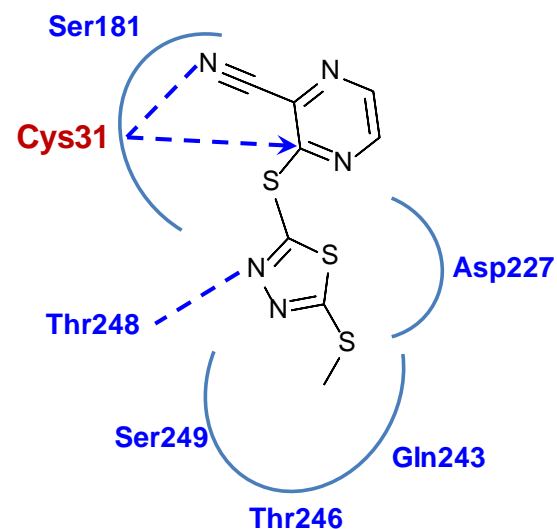
E.

Compound 5



F.

Compound 5



Supplemental Figure 7: Compound A and derivatives docking with LCAT active site. Docking models of Compound A (panel A), Compound 10 (panel C) and Compound 5 (panel E) in the LCAT active site; 2D ligand interaction maps of Compound A (panel B), Compound 10 (panel D) and Compound 5 (panel F). LCAT protein secondary structure is shown in ribbon representation, the active site is depicted by molecular surface in solid mode and colored by lipophilicity. Hydrophilic residues are shown in pink, lipophilic residues are shown in yellow and neutral residues are shown in white. Compounds are shown in ball-and-stick mode. Potential hydrogen-bonds are labeled in dotted lines and selected active site amino acid residues are indicated.